

MECHANISTIC INSIGHTS INTO FOSFOMYCIN RESISTANCE:  
EXAMINATION OF THE FOSX CLASS OF FOSFOMYCIN RESISTANCE PROTEINS

By

Lauren Ashley Beihoffer

Thesis

Submitted to the Faculty of the  
Graduate School of Vanderbilt University

in partial fulfillment of the requirements

for the degree of

MASTER OF SCIENCE

in

Biochemistry

December, 2005

Nashville, Tennessee

Approved:

Professor Richard N. Armstrong

Professor David E. Ong

To my family for their love, support, and compassion

and

To my husband Jim, who inspires me everyday.

## ACKNOWLEDGEMENTS

I would like to acknowledge all those who contributed to this work. First of all, this research would not have been possible without the financial support of the National Institute of Health and the Vanderbilt Center in Molecular Toxicology. I am also greatly indebted to my advisor, Professor Richard N. Armstrong, for his great advice and generous support, and for teaching me what a scientist should be. I would also like to thank all of my lab mates, who not only made daily life more fun, but who greatly inspired me with their advice and suggestions. I am especially grateful for the kind help of Dr. Kerry Fillgrove, Dr. Rachel Rigsby, Larry Thompson, and Daniel Brown.

Of course, I could not have been successful during my time as a graduate student without the love and support of my family. I am forever grateful to my wonderful husband Jim, to my loving mother who is also my best friend, and to my brother who taught me to never take a single moment of my life for granted.

## TABLE OF CONTENTS

	Page
DEDICATION .....	ii
ACKNOWLEDGEMENTS .....	iii
LIST OF TABLES .....	vi
LIST OF FIGURES .....	vii
LIST OF ABBREVIATIONS.....	ix
Chapter	
I. INTRODUCTION .....	1
Antibiotics .....	1
Antibiotic resistance .....	2
The antibiotic fosfomycin .....	5
Antimicrobial resistance to fosfomycin .....	7
Fosfomycin resistance proteins .....	9
Evolution of a new enzymatic activity.....	10
Purpose .....	17
II. MATERIALS AND METHODS.....	18
Materials .....	18
Methods.....	18
Expression of <i>B. melitensis</i> FosX.....	18
Purification of <i>B. melitensis</i> FosX.....	19
ESI mass spectrometry of Purified Protein.....	20
Determination of metal preference by <sup>31</sup> P NMR spectroscopy .....	20
Estimation of the turnover number by <sup>31</sup> P NMR spectroscopy.....	20
Determination of the minimum inhibitory concentration of fosfomycin .....	21
Crystallography of <i>B. melitensis</i> FosX.....	21
Steady state metal binding analysis using fluorescence spectroscopy .....	22
Transient state metal binding analysis using stopped-flow spectroscopy .....	22
Mutant generation .....	22
Expression and purification of mutant <i>M. loti</i> FosX protein .....	23
Activity analysis for mutant <i>M. loti</i> FosX protein .....	23
III. PURIFICATION AND PRELIMINARY CHARACTERIZATION OF THE FOSX ENCODED IN THE GENOME OF <i>BRUCELLA MELITENSIS</i> .....	25
Results.....	25
Expression, purification, and ESI-MS of <i>B. melitensis</i> FosX .....	25
Determination of metal preference by <sup>31</sup> P NMR spectroscopy .....	25

Estimation of the turnover number by $^{31}\text{P}$ NMR spectroscopy.....	28
Determination of the minimum inhibitory concentration of fosfomycin .....	28
X-ray Crystallography .....	31
Discussion .....	32
IV. INVESTIGATION OF METAL BINDING KINETICS FOR FOSX PROTEINS.....	34
Results.....	34
Steady state metal binding analysis .....	34
Transient state metal binding analysis .....	37
Discussion .....	46
V. MUTAGENESIS OF THE CATALYTICALLY TEPID AND PROMISCUOUS FOSX FROM <i>MESORHIZOBIUM LOTI</i> .....	49
Results.....	49
Discussion .....	54
VI. CONCLUSIONS .....	56
APPENDIX .....	59
REFERENCES .....	60

## LIST OF TABLES

Table	Page
1. Antibiotic Families and Their Mechanisms of Action.....	2
2. Timeline of Antibiotic Discovery, Introduction, and Development of Resistance.....	3
3. The Three Classes of Fosfomycin Resistance Proteins: FosA, FosB, FosX .....	8
4. Members of the VOC Superfamily .....	10
5. Catalytic Activity and MIC Values for FosX Enzymes .....	12
6. Summary of Results for MIC Experiments .....	30
7. Dissociation Binding Constants for Metal Binding to FosX Proteins.....	36
8. Observed Off Rate Constants for Metal Binding.....	45
9. Summary of Metal Binding Dissociation Constants for the FosX Proteins.....	45
10. Summary of Catalytic Activity for the Different <i>M. luti</i> FosX Mutants.....	54

## LIST OF FIGURES

Figure	Page
1. The bacterial targets of the major classes of antibiotics: cell wall biosynthesis, protein synthesis, and DNA replication/repair .....	1
2. Acquisition and mechanisms of bacterial resistance .....	4
3. The structure of fosfomycin .....	5
4. MurA (UDP-N-acetylglucosamine-3-enolpyruvyltransferase) catalyzes the enol ether transferase of PEP to UDP-GlcNAc, the first committed step in cell wall biosynthesis .....	6
5. The inactivation of MurA involves the alkylation of a critical cysteine residue.....	7
6. Reactions catalyzed by the three classes of fosfomycin resistance proteins .....	9
7. The <i>M. luti</i> FosX is a promiscuous enzyme.....	11
8. The threshold model of evolution.....	13
9. Overlay of FosA and FosX active sites .....	14
10. Structural comparison of FosX and FosA proteins .....	16
11. Purification of <i>B. melitensis</i> FosX yields pure protein of the correct molecular weight.....	26
12. Catalytic activity of the <i>B. melitensis</i> FosX in the presence of various divalent metal cations.....	27
13. <sup>31</sup> P NMR spectrum of a reaction mixture showing approximately 10% conversion of substrate into product .....	28
14. Bacterial growth and resistance on LB plates containing fosfomycin .....	29
15. Induction of protein expression does not significantly alter the MIC value for <i>B. melitensis</i> FosX .....	30
16. Cells transformed with the <i>B. melitensis</i> expression vectogr and grown in the presence of copper do not have increased MIC values .....	31
17. Protein crystals of <i>B. melitensis</i> FosX.....	32

18. Steady state analysis of metal binding to the FosX proteins: relative change in intrinsic protein fluorescence at 335 nm upon metal titration of (a) <i>L. monocytogenes</i> FosX, (b, c) <i>B. melitensis</i> FosX, (d, e) <i>C. botulinum</i> FosX .....	35
19. Diagram illustrating the stopped-flow experimental design used to determine $k_{on}$ and $k_{off}$ and the apparent equilibrium dissociation constant .....	37
20. Stopped flow analysis of $Cu^{2+}$ binding to <i>B. melitensis</i> FosX reveals a two step process .....	38
21. Stopped flow analysis of $Mn^{2+}$ binding to <i>B. melitensis</i> FosX reveals a two step process .....	39
22. Stopped flow analysis of $Cu^{2+}$ binding to <i>C. botulinum</i> FosX reveals a two step process .....	40
23. Stopped flow analysis of $Mn^{2+}$ binding to <i>C. botulinum</i> FosX reveals a two step process .....	41
24. Stopped flow analysis of $Mn^{2+}$ binding to <i>L. monocytogenes</i> FosX reveals a two step process .....	42
25. Diagram illustrating the stopped-flow experimental design used to observe $k_{off}$ directly .....	43
26. Stopped-flow data traces observed upon rapid mixing of the enzyme-metal complex with EDTA.....	44
27. Sequence alignment of FosA $K^+$ loop with FosX .....	49
28. Activity of <i>M. loti</i> FosX containing mutations for a $K^+$ binding loop .....	51
29. Activity of <i>M. loti</i> FosX containing the $K^+$ loop mutations and E44G/F46Y/M57S mutant background .....	52
30. Sequence alignment and computational modeling reveal residues that need to be mutated in <i>M. loti</i> FosX to enhance GSH binding.....	53



## LIST OF ABBREVIATIONS

DNA	Deoxyribonucleic acid
MurA	Uridine-5'-diphospho- <i>N</i> -acetyl-D-glucosamine-3-enolpyruvyltransferase
PEP	Phosphoenolpyruvate
UDP-GlcNAc	Uridine-5'-diphospho- <i>N</i> -acetyl-D-glucosamine
GSH	Glutathione
GST	Glutathione- <i>S</i> -transferase
VOC	Vicinal oxygen chelate
LB	Luria-Bertani Media
MIC	Minimum inhibitory concentration
IPTG	Isopropyl- $\beta$ -D-thiogalactopyranoside
DTT	Dithiothreitol
EDTA	Ethylenediamine tetraacetic acid
TRIS	Tris(hydroxymethyl)aminomethane
HEPES	N-(2-hydroxyethyl)piperazine N'-(2-ethanesulfonic acid)
MOPS	3-(N-morpholino)-propanesulfonic acid
DEAE	Diethylaminoethyl
TMA	Tetramethylammonium
OD <sub>600</sub>	Optical density at 600 nm
NMR	Nuclear magnetic resonance
ESI-MS	Electrospray ionization mass spectrometry
SDS-PAGE	Sodium dodecyl sulfate-polyacrylamide gel electrophoresis

# CHAPTER I

## INTRODUCTION

### Antibiotics

Prior to the 1930's, bacterial infections were the major cause of death in humans (1). Consequently, the discovery and development of compounds capable of inhibiting microbial growth was a major milestone in the history of medicine. These compounds, termed antibiotics, were first introduced into the clinical setting over 60 years ago, and since that time, have remained the primary treatment for bacterial diseases.

Antibiotics function to kill pathogenic bacteria by selectively targeting processes necessary for bacterial growth and survival, with the main targets being cell wall biosynthesis, protein synthesis, and DNA replication and repair (Figure 1). The major families of antibiotics that utilize these mechanisms are shown in Table 1.

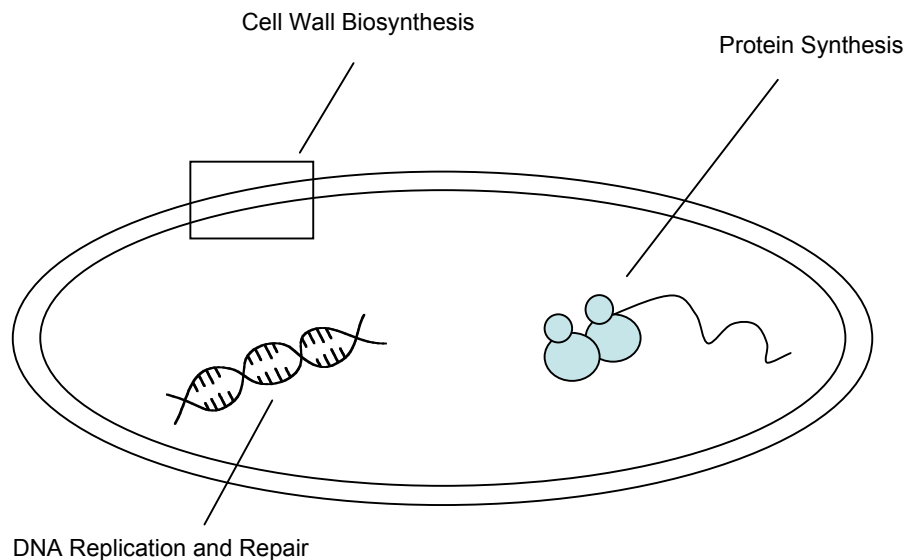


**Figure 1.** The bacterial targets of the major classes of antibiotics: cell wall biosynthesis, protein synthesis, and DNA replication/repair.

**Table 1.** Antibiotic Families and Their Mechanisms of Action

<b>Major Antibiotic Families</b>	<b>Mechanism of Action</b>
Penicillin, cephalosporins, carbapenems, daptomycin, monobactams, glycopeptides	Inhibition of cell wall synthesis
Tetracyclines, aminoglycosides, oxazolidonones, streptogramins, ketolides, macrolides, lincosamides	Inhibition of protein synthesis
Fluoroquinolones	Inhibition of DNA synthesis

Although antibiotics were initially triumphantly successful in treating diseases once thought to be incurable—such as tuberculosis and pneumonia—their efficacy has been compromised by the rapid appearance of antimicrobial resistance.

#### Antibiotic Resistance

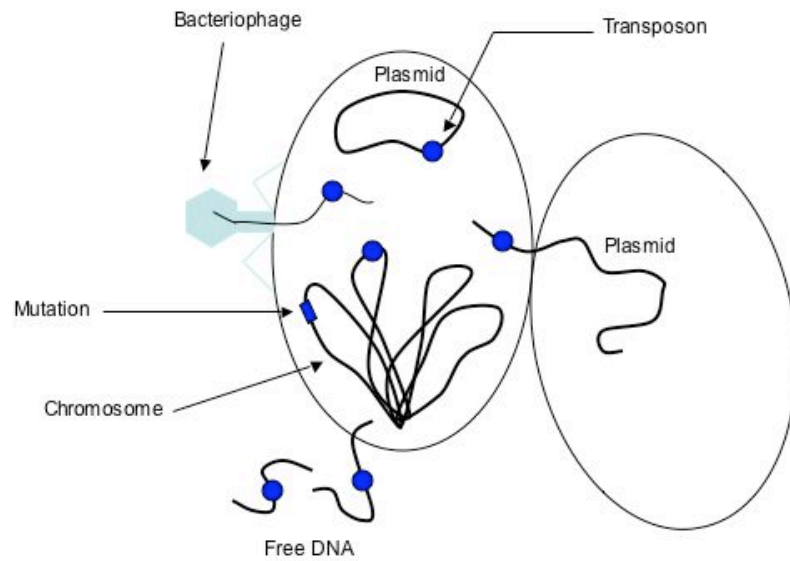
Unfortunately, bacteria are constantly developing strategies by which to combat the action of antibiotics (2). Antibiotic resistance usually emerges quickly after introduction of the drug into the clinic and consistently appears as new drugs are introduced (3) (Table 2). In fact, drug discovery and development are disproportionate to the sharp increase in antibiotic resistance seen in the last decade. Consequently, it is important to understand the mechanisms by which bacteria develop antibiotic resistance so that new strategies to combat pathogens can be pursued.

**Table 2.** Timeline of Antibiotic Discovery, Introduction, and Development of Resistance

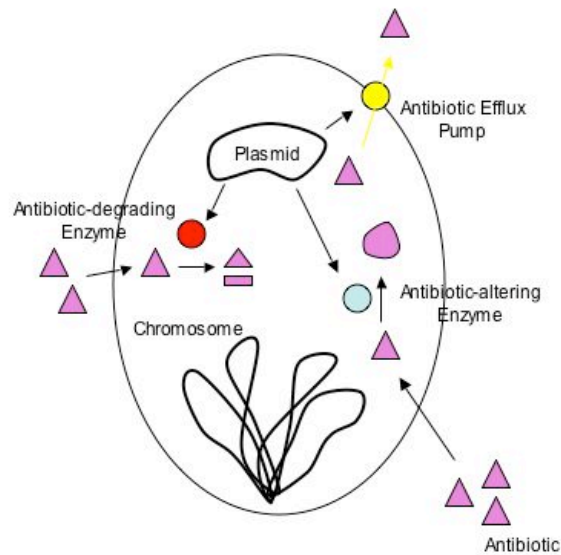
<b>Antibiotic</b>	<b>Year Discovered</b>	<b>Year Introduced</b>	<b>Year Resistance Identified</b>
Penicillin	1929	1940	1943
Streptomycin	1944	1947	1947
Tetracycline	1948	1952	1956
Erythromycin	1952	1955	1956
Vancomycin	1956	1972	1987

Antibiotic resistance is not a novel occurrence, but the problem is expanding at an alarming rate, being fueled partly by an increase in antimicrobial usage. Each year, millions of kilograms of antibiotics are used to treat people as well as animals and agriculture. The over-usage and inappropriate usage of antibiotics helps propagate resistance by killing strains that are susceptible to the drug while selecting for strains that are resistant, thus giving the resistant bacteria the opportunity to spread and multiply in the presence of a selective pressure (5).

There are several ways in which bacteria can become resistant to a particular antibiotic. Bacteria can acquire antibiotic resistance through mobile genetic elements, such as plasmids, transposons, or bacteriophages, which carry genes sufficient for resistance to a particular antibiotic. Alternatively, step-wise mutations in chromosomal genes can be used as a method for acquiring drug resistance (Figure 2a). The mechanism of resistance typically utilizes one of three strategies: enzymatic alteration or degradation of the antibiotic, alteration of the drug target, or alteration of drug uptake or export from the cell (Figure 2b) (5).



a.



b.

**Figure 2.** Acquisition and mechanisms of bacterial resistance. (a) Bacteria may acquire resistance to an antibiotic by several different mechanisms: Chromosomal mutation or obtainment of foreign DNA by transposons, bacteriophages, plasmids, or free DNA. (b) Strategies utilized by bacteria for resistance to antibiotics: antibiotic degrading enzymes, antibiotic altering enzymes, and antibiotic efflux pumps.

The startling effect of antibiotic resistance was made apparent in 1994 when bacteria isolated from hospital patients were found to be concurrently resistant to all available antibiotics. This type of multi-drug resistance has become an alarming problem in pathogens such as *Staphylococcus aureus*, *Streptococcus pneumoniae*, and *Salmonella enterica*. Although there are 15 distinct classes of antibiotics, each has been susceptible to some form of resistance. Even antibiotics that are considered to be the last line of defense--the fluoroquinolones, vancomycin and carbapenems--have not escaped resistance by pathogens capable of deadly infection (5). Further complicating the issue is the fact that there has been only one new class of antibiotics introduced in the last 40 years, and the small number of new prospects includes only modified versions of drugs already in use. Furthermore, it appears that the resistance problem will not be entirely solved by the development of new antibiotics, since none so far have evaded resistance. Antimicrobial resistance has been estimated to cost the United States up to \$24 billion a year, and in 1992 it was ranked the 11<sup>th</sup> leading cause of death in the United States (3).

#### The Antibiotic Fosfomycin

Fosfomycin, (1*R*, 2*S*)-epoxypropylphosphonic acid (Figure 3), is an extremely stable natural product produced by strains of the soil-dwelling bacteria *Streptomyces*.

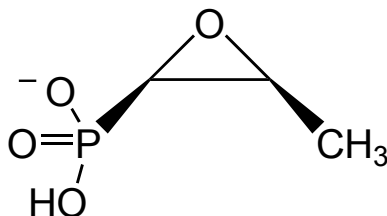


**Figure 3.** The structure of fosfomycin

Fosfomycin was first identified by Merck Research Laboratories in 1969 and was shown to be a very effective antimicrobial agent, possessing broad-spectrum antibacterial activity against both Gram-positive and Gram-negative bacteria. Fosfomycin demonstrates many pharmacologically desirable properties such as good bioavailability, low metabolism, and lack of toxicity in humans due to no human target (6). The mechanism of action of fosfomycin involves the inactivation of MurA (UDP-N-acetylglucosamine-3-enolpyruvyltransferase), an enzyme necessary for the first committed step in cell wall biosynthesis. Specifically, MurA catalyzes the enol ether transfer of PEP to UDP-GlcNAc (7) (Figure 4).

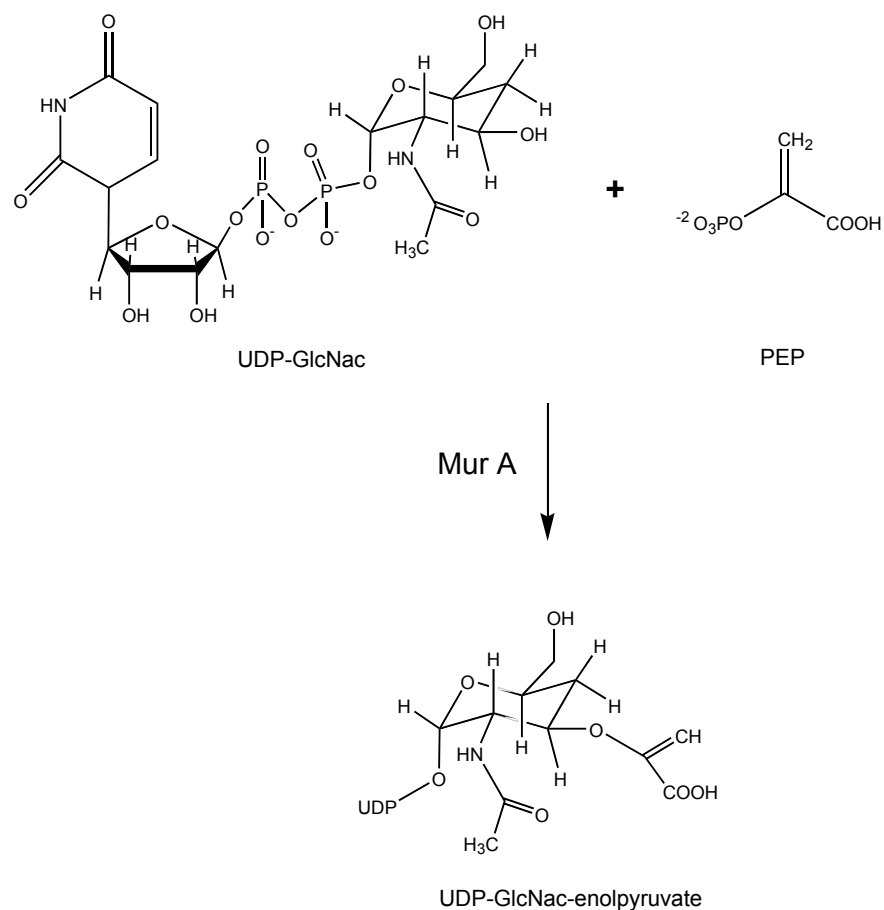


**Figure 4.** MurA (UDP-N-acetylglucosamine-3-enolpyruvyltransferase) catalyzes the enol ether transfer of PEP to UDP-GlcNAc, the first committed step in cell wall biosynthesis.

Fosfomycin acts as a substrate analogue of phosphoenolpyruvate and renders the MurA enzyme inactive through alkylation of an active site cysteine residue (7) (Figure 5).

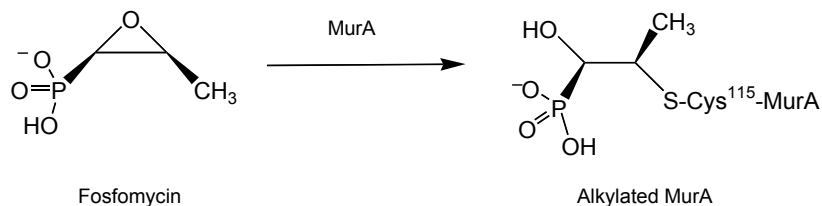


**Figure 5.** The inactivation of MurA involves the alkylation of a critical cysteine residue.

Fosfomycin is currently used to treat lower urinary tract infections and is classified as a category B drug by the FDA, indicating that it is suitable for use during pregnancy (8). In addition, it has been demonstrated that fosfomycin has the potential to be useful in combinational therapies for treating vancomycin-resistant enterococcal infections (9) as well as quinolone-resistant strains of *E. coli* (10), indicating that fosfomycin is an important and useful antibiotic. Unfortunately, fosfomycin is not exempt from the mounting resistance problem.

#### Antimicrobial Resistance to Fosfomycin

Resistance to fosfomycin has developed through three different mechanisms; alteration of the drug target MurA (11), alteration of fosfomycin uptake into cells (12,13), and enzymatic modification and inactivation of the drug by fosfomycin resistance proteins (14). Enzymes that directly modify and inactivate antibiotics, such as the fosfomycin resistance proteins, are particularly interesting since they serve as potential targets for the design of inhibitors.



## Fosfomycin Resistance Proteins

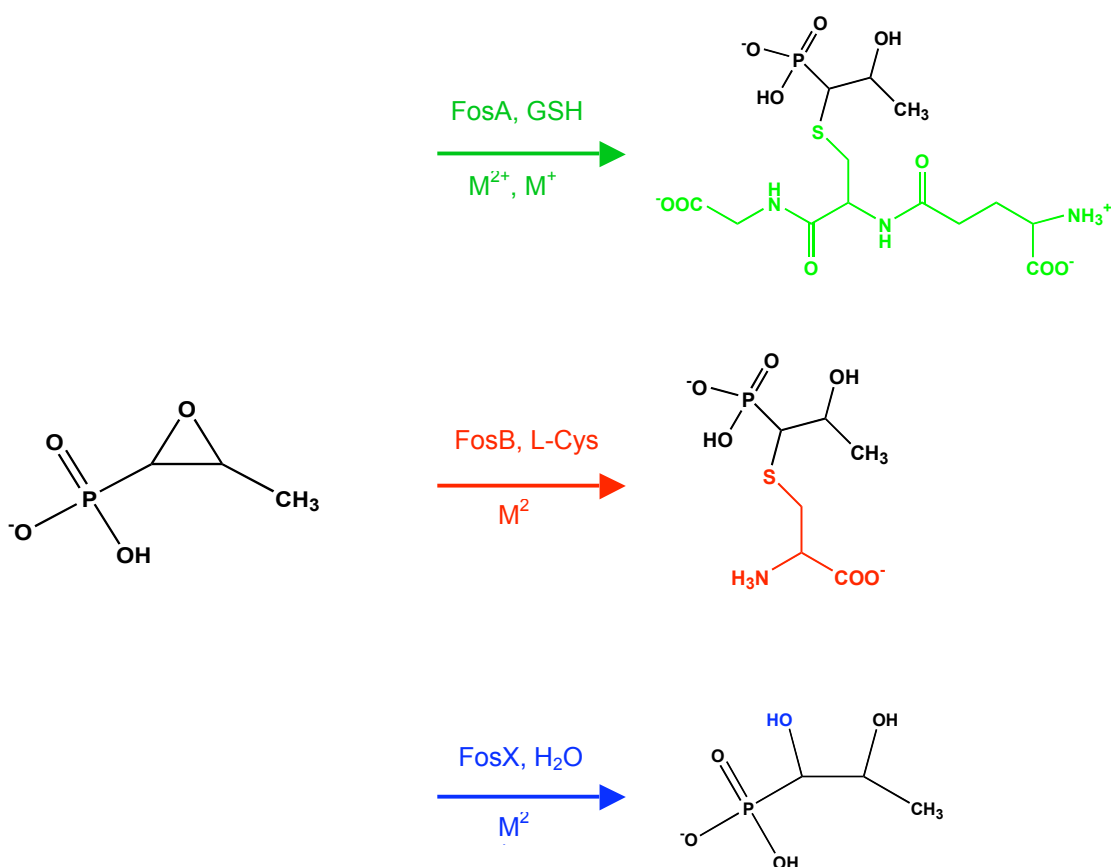
Plasmid-encoded resistance to the antibiotic fosfomycin was first observed in the clinic in 1982 after isolation of the transposon Tn2921 from *Serratia marcescens* (14). The gene responsible for resistance was later found to encode a 16 kDa glutathione S-transferase (GST), designated FosA, that inactivates fosfomycin through covalent attachment of the tri-peptide glutathione (GSH) (15, 16). This particular GST was not related to the canonical GST's, but BLAST searches of microbial genomes revealed several genomically encoded proteins possessing high homology to the FosA enzyme. These enzymes were termed fosfomycin resistance proteins. The genomically encoded fosfomycin resistance proteins segregated into three classes based on sequence identity and type of reaction catalyzed (Figure 6). They are designated FosA, FosB, and FosX (Table 3).

**Table 3.** The Three Classes of Fosfomycin Resistance Proteins: FosA, FosB, and FosX

	Gene Origin	% Identity		
		FosA	B	X
FosA	Transposon Tn2921 (plasmid)	100	37	28
	<i>Pseudomonas aeruginosa</i> PA1129	60	36	29
	<i>Pseudomonas fluorescens</i>	57	40	28
	<i>Nostoc. Sp.</i>	51	37	30
FosB	<i>Staphylococcus epidermidis</i>	37	100	30
	<i>Staphylococcus aureus</i>	36	68	28
	<i>Bacillus subtilis</i>	33	63	33
	<i>Bacillus halodurans</i>	38	61	32
	<i>Bacillus anthraxis</i>	39	59	32
FosX	<i>Mesorhizobium loti</i> mlr3345	28	30	100
	<i>Brucella melitensis</i>	28	28	62
	<i>Clostridium botulinum</i>	23	32	47
	<i>Listeria monocytogenes</i>	30	33	59

## Fosfomycin Resistance Proteins

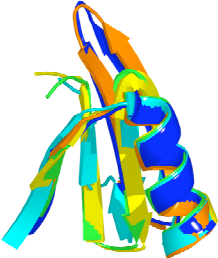
The FosA enzymes are manganese-dependent glutathione S-transferases that catalyze the nucleophilic addition of the tripeptide GSH to C<sub>1</sub> of fosfomycin, opening the epoxide ring and rendering the drug inactive. These enzymes show 100-fold activation in the presence of a monovalent cation such as potassium (18, 19). The FosB enzymes are magnesium-dependent thiol-transferases that catalyze the addition of L-cysteine to fosfomycin. The more distantly related FosX proteins are epoxide hydrolases that catalyze the addition of water to C<sub>1</sub> of fosfomycin, giving rise to a diol product (21). The FosX enzymes also possess a divalent metal ion requirement.



**Figure 6.** Reactions catalyzed by the three classes of fosfomycin resistance proteins.

Fosfomycin resistance proteins belong to the Vicinal Oxygen Chelate (VOC) superfamily, which is composed of structurally related metalloenzymes that catalyze diverse reactions. All members share a paired  $\beta\alpha\beta\beta$  motif, which forms the basic structural unit of this family. The superfamily includes enzymes such as glyoxylase I, extradiol dioxygenase, bleomycin resistance protein, and methylmalonyl-CoA epimerase, all proposed to have arisen from a common progenitor (17) (Table 4).

**Table 4:** Members of the VOC Superfamily

	Member	Reaction Catalyzed
 <p><math>\beta\alpha\beta\beta</math> motif</p>	<b>Fosfomycin Resistance Protein</b>	Nucleophilic opening of epoxide
	<b>Bleomycin Resistance Protein</b>	None (sequestration)
	<b>Extradiol Dioxygenase</b>	Oxidative cleavage of C-C bond
	<b>Glyoxalase I</b>	Isomerization
	<b>Methylmalonyl-CoA Epimerase</b>	Epimerization

#### Evolution of a New Enzymatic Activity

Kinetic characterization of the FosA encoded by the transposon *Tn2921* has revealed that this highly efficient enzyme not only provides bacteria with robust resistance to fosfomycin, but has reached kinetic perfection as well, with  $k_{cat}/K_m = (1.4 \pm 0.1) \times 10^7$ . The FosA enzyme encoded by *Pseudomonas aeruginosa* has also been well characterized. Although not as efficient as the *TN2921* FosA, this enzyme does show high catalytic efficiency and provides the native organism with robust resistance to fosfomycin (20). Much less is known about the more distantly related FosX enzymes,

however. Preliminary examination of FosX proteins from a variety of pathogens reveals a wide range of catalytic activity, with all of the FosX enzymes demonstrating much less catalytic efficiency than the FosA's (Table 5) (21). For example, the FosX enzyme encoded in the genome of *Listeria monocytogenes* shows proficient catalytic activity and nearly all *Listeria* clinical isolates are inherently resistant to fosfomycin, indicating that the *L. monocytogenes* FosX enzyme is functioning as an antibiotic resistance protein in this organism (22). Alternatively, the FosX from *M. loti*, which is not even a human pathogen, has very poor catalytic activity and there is no evidence of inherent fosfomycin resistance in this organism. Additionally, the *M. loti* enzyme has demonstrated the ability to catalyze the FosA reaction at very low levels in addition to the FosX reaction for which it is classified (Figure 7).

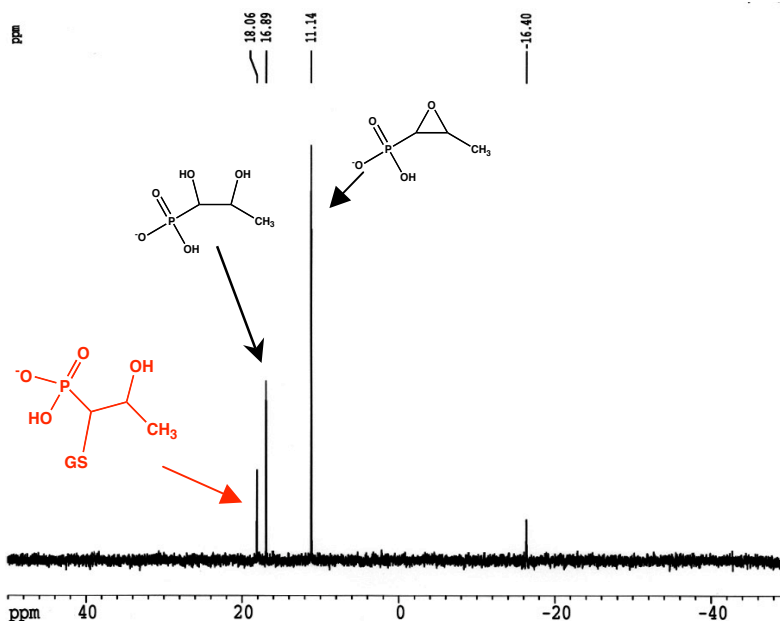


**Figure 7.** The *M. loti* FosX is a promiscuous enzyme.  $^{31}\text{P}$  NMR shows that it is able to form both the FosX diol product (16.89 ppm) and the FosA GSH-conjugated product (18.06 ppm) upon incubation with substrates fosfomycin (11.14 ppm) and GSH.

This catalytically promiscuous enzyme has low catalytic efficiency for either reaction. Additionally, the gene encoding the *M. loti* FosX appears to be in a phosphonate utilization operon, indicating that it may possess an alternate biological role in the *M. loti* organism. It can even be suggested that the *M. loti* FosX is an intermediate in the evolution of the fosfomycin resistance proteins. Accordingly, when expressed in *E. coli*, the *L. monocytogenes* FosX enzyme can confer robust resistance to fosfomycin while the *M. loti* enzyme cannot confer significant resistance in the biological context of *E. coli* (21). These observations (Table 5) suggest that this catalytically poor FosX protein may possess uncharacterized activity representing its true biological function in the native organism.

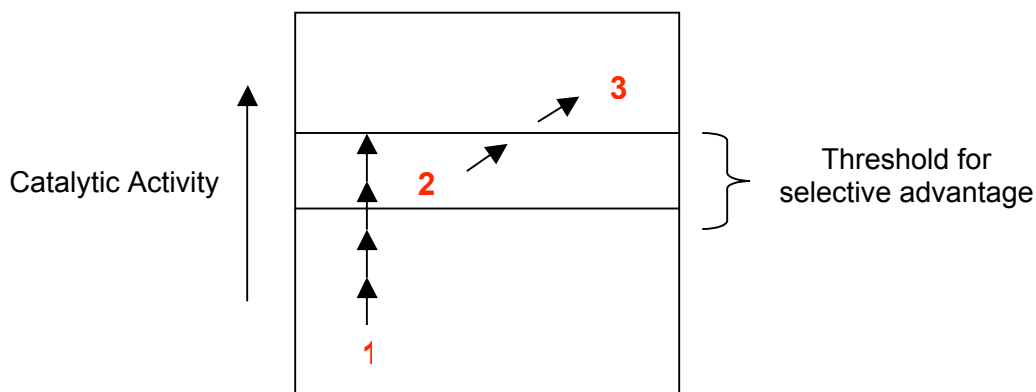
**Table 5.** Catalytic Activity and MIC Values for FosX Enzymes

Enzyme	$k_{cat}/K_m$ ( $M^{-1}s^{-1}$ )	Promiscuity (FosA Activity)	MIC* (mg/mL Fos.)
TN2921 FosA	$(1.4 \pm 0.1) \times 10^7$	No	> 25
<i>P. aeruginosa</i> FosA	$(9.0 \pm 1.4) \times 10^5$	No	> 25
<i>L. monocytogenes</i> FosX	$(9.0 \pm 2.0) \times 10^4$	No	>25
<i>M. loti</i> FosX	$(5.0 \pm 0.6) \times 10^2$	Yes ( $0.006 s^{-1}$ )	< 0.025

\*MIC is the minimum inhibitory concentration of fosfomycin when protein is expressed in *E. coli*.

It is possible that fosfomycin resistance proteins originated from detoxication enzymes or phosphonate utilization enzymes which underwent mutation to generate altered catalytic ability for survival in the presence of fosfomycin. It is important to emphasize the fact that fosfomycin is a natural product produced by soil microbes for self-defense against other pathogens, meaning that exposure of bacteria to this compound is not a recent, man-made occurrence. The possibility that the *M. loti* FosX is an intermediates in the catalytic alteration of a progenitory enzyme is supported by the

observation of catalytic promiscuity and weak catalytic activity of *M. loti* FosX. This concept can be rationalized by the threshold model of evolution for generation of a new enzymatic activity. The evolution of a new enzymatic activity has been suggested to occur through gene duplication and adaptive evolution events, resulting in enzyme superfamilies (like the VOC family) that share common mechanistic features but that catalyze very diverse reactions. Catalytic promiscuity may play a role in this process by conferring a selective advantage to a duplicated gene. Several enzymes have demonstrated the ability to catalyze alternative reactions at very low levels, with these alternative activities being separate and distinct from the native biological reactions catalyzed by the enzymes. A duplicated gene possessing promiscuous activity at an appropriate level may offer a selective advantage that would encourage the development of a novel enzymatic activity. This hypothesis is presented as a threshold model for evolution of a new activity (Figure 8) (23).



**Evolutionary Starting Points:**

- 1 = Inactive progenitor: many mutations required
- 2 = Promiscuous progenitor: few mutations required
- 3 = Promiscuous progenitor: no mutations required

**Figure 8** The threshold model of evolution. (Adapted from O'Brien, P., *et al.* (1999) *Chemistry & Biology*, 6, R91-R105).

Preliminary observations of FosX activity gave rise to site-directed mutagenesis experiments in order to identify residues critical for proficient catalytic activity as well as those involved in converting promiscuous FosX activity into the proficient, evolutionarily advanced FosA activity. Examination of protein crystal structures and initial mutagenesis experiments have revealed a conserved active site glutamate (the corresponding residue in FosA is a glycine) that plays a vital role in catalysis, possibly acting as a general base to facilitate addition of water to fosfomycin (Figure 9). Mutating this residue to glycine virtually abolishes the catalytic activity of the enzyme (21).

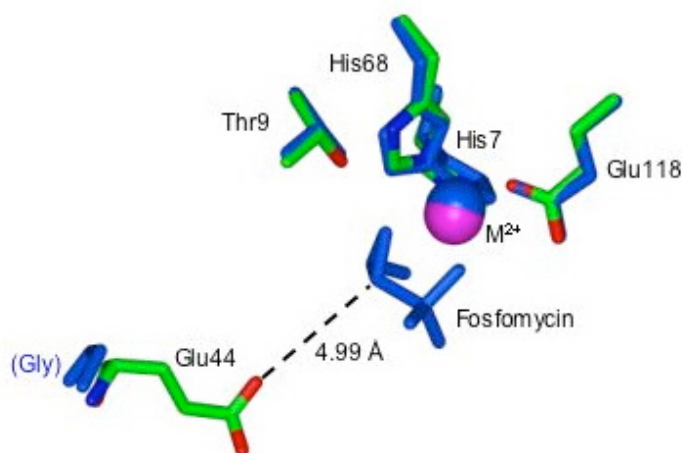


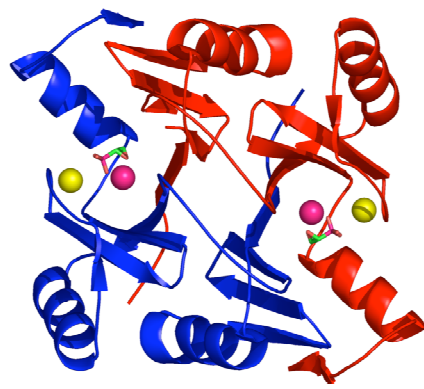
**Figure 9.** Overlay of FosA and FosX active sites. Blue residues indicate FosA residues, while the multi-colored residues represent the FosX protein. Note that the fosfomycin is present in the FosA structure only.

In the *M. loti* FosX, the mutation of E44G was made in addition to two more active site residues, F46Y and M57S, which amazingly not only abolished FosX activity, but increased the promiscuous FosA activity of this enzyme 250-fold (Fillgrove, unpublished

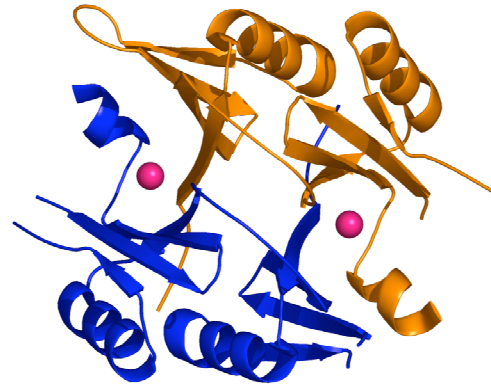
data). This triple mutant inspired closer structural examination of FosA and FosX proteins to reveal residues that are important and distinct for FosA versus FosX activity.

Comparison of crystal structures of FosA and FosX proteins (Figure 10a) reveals the presence of a potassium-binding loop in FosA that is absent in FosX (Figure 10b) (21). Although the role of the potassium-binding loop in catalysis is not completely clear, the residues comprising the loop are of particular interest for mutagenesis in both the FosA and FosX proteins. It is known that potassium provides 100-fold activation for FosA catalysis, and it is expected that insertion of the loop into FosX through site-directed mutagenesis will yield similar activation. Additionally, computational modeling was used to dock GSH onto the crystal structure of the *P. aeruginosa* FosA, revealing residues that may be important for GSH binding in this enzyme. This information will also play a role in mutagenesis experiments aimed at transforming *M. loti* FosX's promiscuous activity into a proficient FosA activity.



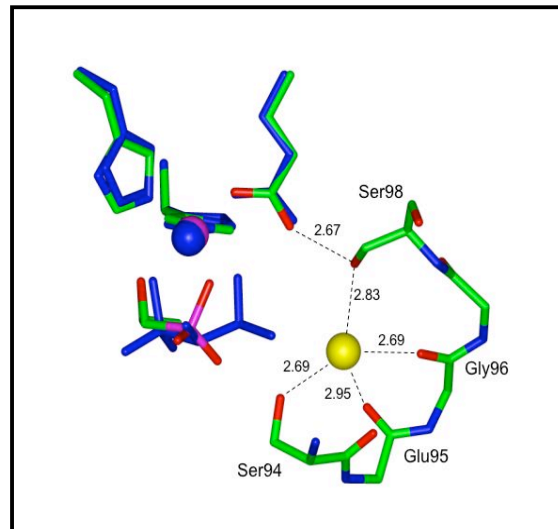
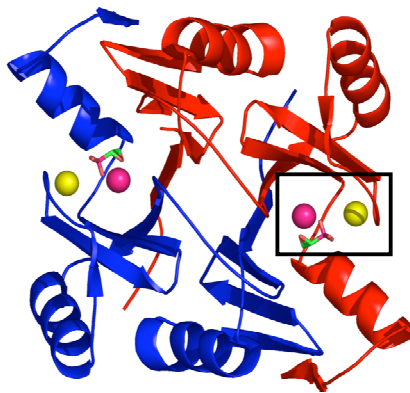


FosA



FosX

a



b

**Figure 10.** Structural comparison of FosX and FosA proteins. (a) Ribbon diagrams of the FosA from *Pseudomonas aeruginosa* and the FosX from *Mesorhizobium loti*. (b) Diagram illustrating the residues forming the K<sup>+</sup> binding loop in FosA proteins.

## Purpose

As the antimicrobial resistance problem continues to escalate, there is a critical need for the development of novel therapies to combat resistant, life-threatening microbes. A comprehensive understanding of the molecular basis of resistance will aid the development of new strategies to treat bacterial infections. Furthermore, enzymes that directly modify and inactivate antibiotics are particularly interesting since they serve as potential targets for inhibitors. The goal of this work was to study the enzymology of the antibiotic-altering FosX protein from the human pathogen *Brucella melitensis* and from the soil microbe *Mesorhizobium loti* in order to gain a better understanding of genomically-encoded fosfomycin resistance.

## CHAPTER II

### MATERIALS AND METHODS

#### Materials

*Escherichia coli* BL21(DE3) cells were from Novagen (Madison, WI). Isopropyl- $\beta$ -D-thiogalactopyranoside (IPTG) and dithiothreitol (DTT) were from RPI (Mt. Prospect, IL). Ampicillin, protease inhibitor cocktail, lysozyme, streptomycin sulfate, potassium phosphate, ethylenediamine tetraacetic acid (EDTA), tris(hydroxymethyl)aminomethane (TRIS), N-(2-hydroxyethyl)piperazine N'-(2-ethanesulfonic acid) (HEPES), 3-(N-morpholino)-propanesulfonic acid (MOPS), and glutathione were from Sigma (St. Louis, MO). Fosfomicin was from Fluka (Ronkonkoma, NY). Hydroxylapatite resin and Chelex 100 resin were from BioRad. DEAE Fast Flow resin was from Amersham Biosciences (Uppsala, Sweden). Metals (puratronic grade), as their chloride salts, were from Alfa Aesar (Ward Hill, MA). Tetramethylammonium hydroxide (TMAOH) was from Acros. QuikChange Site-Directed Mutagenesis Kit was from Stratagene (La Jolla, CA) and Wizard *Plus* Minipreps DNA Purification System was from Promega (Madison, WI). Crystallization screens were from Hampton Research and deCODE Genetics.

#### Methods

##### *Expression of B. melitensis FosX*

*E. coli* BL21(DE3) cells were transformed with a pET-20b expression vector containing the gene encoding *B. melitensis* FosX. Four 2 L cultures were inoculated with bacteria from starter cultures to reach a starting  $OD_{600} = 0.015$ . The bacteria were

grown at 37°C with shaking at 225 rpm until an OD<sub>600</sub> = 0.8 was reached. At this point, cultures were induced with 600 μM IPTG to stimulate protein expression. Bacteria allowed to express protein for four hours. Cells then harvested by centrifugation and stored at -80°C.

#### *Purification of B. melitensis FosX*

Cell pellets were thawed on ice and resuspended in 75 mL 25mM Tris buffer, pH 8.2 (buffer A). To aid cell lysis, 0.1 mg/mL lysozyme was added and cells incubated at room temperature for 20 minutes with gentle rocking, then incubated on ice for 30 minutes. Protease inhibitor cocktail was added and the cells were lysed by sonication. Cellular debris was removed by centrifugation (30,000 x g for 25 min). Nucleic acids were then precipitated and removed from the cleared lysate by the addition of 700 mg streptomycin sulfate dissolved in 2 mL H<sub>2</sub>O, followed by centrifugation (30,000 x g for 25 min.) Crude lysate was dialyzed against buffer A (all dialysis performed at 4°C and in the presence of 0.5 mM DTT). Crude lysate was then passed through a DEAE fast flow column (2.5 x 13 cm) equilibrated with buffer A. Column was washed with buffer A and protein was eluted using a linear NaCl gradient (25-400 mM). Fractions containing *B. melitensis* FosX protein were identified by absorbance at 280 nm and SDS-PAGE analysis. Fractions containing the protein were pooled and placed into dialysis against buffer B (25 mM potassium phosphate, pH 7.5), and then dialyzed against buffer C (25 mM potassium phosphate, pH 6.8). Protein was then passed through an HA column (1.5 x 16 cm) equilibrated with buffer C. Protein was isocratically eluted with buffer C and the collected protein was dialyzed against the first demetalation buffer, buffer D (20 mM Mops pH 6.8, 100 mM NaCl, 5 mM EDTA, 3 g chelex resin). Protein was then dialyzed against the second demetalation buffer, buffer E (25 mM TMA-Hepes pH 7.0,

10 mM NaCl, 3 g chelex resin) , followed by dialysis in buffer F (25 mM TMA-Hepes, pH 7.5). Protein was concentrated using a nitrogen pressure cell and an Amicon 10K molecular weight cut-off membrane. Protein was aliquoted, flash-frozen on dry ice then immediately stored at -80°C.

#### *ESI Mass Spectrometry of Purified Protein*

For ESI-MS analysis, 2 pmol/ $\mu$ L protein was prepared in a 1:1 solution of H<sub>2</sub>O/ACN with 1% acetic acid. Sample was then directly injected into a ThermoFinnigan LCQ ion-trap mass spectrometer (San Jose, CA) in positive-ion mode.

#### *Determination of Metal Preference by <sup>31</sup>P NMR Spectroscopy*

In a typical reaction, 300nM enzyme was allowed to equilibrate with 100  $\mu$ M of metal in 25 mM Hepes, pH 7.5. Reaction was initiated by the addition of 25 mM fosfomycin and allowed to proceed for 20 minutes. Reactions were quenched by the addition of 50  $\mu$ L CHCl<sub>3</sub> and vigorous vortexing, followed by immediate freezing on dry ice. Reactions were thawed and then centrifuged to pellet and remove precipitated protein. The aqueous layer was demetalated with chelex resin for 3 hours. Chelex resin was pelleted and removed and the remaining aqueous layer was used for NMR analysis after the addition of D<sub>2</sub>O. Proton-decoupled <sup>31</sup>P spectra of the reactions were collected at 121 MHz, with <sup>31</sup>P chemical shifts of 16.9 ppm for diol product and 11.1 ppm for fosfomycin.

#### *Estimation of the Turnover Number by <sup>31</sup>P NMR Spectroscopy*

In a typical reaction, 500nM enzyme was allowed to equilibrate with 100  $\mu$ M metal in 25 mM Hepes, pH 7.5. Reaction was initiated by the addition of 25 mM

Fosfomycin and allowed to proceed for several minutes. Reactions were quenched by the addition of 50  $\mu\text{L}$   $\text{CHCl}_3$  and vigorous vortexing, followed by immediate freezing on dry ice. Reactions thawed and centrifuged to pellet and remove precipitated protein. The aqueous layer was demetalated with chelex resin for 3 hours. Chelex resin was pelleted and removed and the remaining aqueous layer was used for NMR analysis after the addition of  $\text{D}_2\text{O}$ . Proton-decoupled  $^{31}\text{P}$  spectra of the reactions were collected at 121 MHz. The amount of product formed was then determined from the ratio of peak heights (for substrate and product) and the amount of substrate used in the reaction, and this information was used to estimate the turnover for the enzyme.

#### *Determination of the Minimum Inhibitory Concentration of Fosfomycin*

*E. coli* BL21(DE3) cells containing the appropriate expression plasmid were used to determine the MIC of fosfomycin for various FosX proteins. Cells containing the empty expression plasmid were used as a control. Bacteria of  $\text{OD}_{600} = 0.015$  were streaked onto LB-agar plates containing 100  $\mu\text{g}/\text{mL}$  ampicillin, 30  $\mu\text{M}$  glucose-6-phosphate, and various concentrations of fosfomycin (0-5.0 mg/mL). Plates were incubated at 37°C for 16 hours and bacterial growth was recorded and photographed.

#### *Crystallography*

Protein crystallization screens for *B. melitensis* FosX protein were performed using the hanging drop vapor diffusion method using Hampton screens 1 and 2, Hampton Index screens (Hampton Research), and Wizard screens 1 and 2 (deCODE Genetics). Protein concentrations ranged from 8 mg/mL to 16 mg/mL. Metal (Cu(II) or Mn (II)) and fosfomycin were used in some screens.

### *Steady State Metal Binding Analysis using Fluorescence Spectroscopy*

In order to determine the dissociation constant,  $K_D$ , for metal binding, enzyme was titrated with increasing amounts of metal in order to observe changes in intrinsic protein fluorescence. In a typical experiment, 100 nM enzyme was mixed with increasing amounts of metal (usual concentration range was from 200 nM to 3.0  $\mu$ M). The enzyme-metal complex was excited at 275 nm and fluorescence was observed at 335 nm in a Horiba Fluorolog.  $K_D$  was then determined from a plot of relative fluorescence versus concentration of metal.

### *Transient State Metal Binding Analysis using Stopped-Flow Spectroscopy*

In a typical stopped-flow experiment, 400 nM enzyme was mixed rapidly with metal (ranging in concentration from 1.2  $\mu$ M to 180  $\mu$ M) in an Applied Photophysics SX17 stopped-flow spectrometer set in fluorescence mode. The final concentration of enzyme in the observation cell was 200 nM. The excitation wavelength was 275 nm and fluorescence emission was observed above 320 nm. Data were fit to a double exponential and  $k_{obs}$  values were obtained. Using the  $k_{obs}$  values, on and off rates for metal binding, as well as apparent dissociation constants for metal binding, were determined.

### *Mutant Generation*

The QuikChange site-directed mutagenesis kit (Promega) was used in conjunction with synthetic oligonucleotide primers (Life Technologies) and PCR to mutate the *M. loti* FosX expression plasmid.

### *Expression and Purification of Mutant M. loti FosX Protein*

Mutant protein was expressed the same as for the *B. melitensis* FosX described above. Purification was essentially the same as above but with minor modifications. Cell pellets were thawed on ice and resuspended in 75 mL 25mM Tris buffer, pH. 7.5 (buffer A). Lysozyme (0.1 mg/mL) was added and cells incubated at room temperature for 20 minutes with gentle rocking, then incubated on ice for 30 minutes. Protease inhibitor cocktail was added and the cells were lysed by sonication. Cellular debris was removed by centrifugation (30,000 x g for 25 min). Nucleic acids were then precipitated and removed from the cleared lysate by the addition of 700 mg streptomycin sulfate dissolved in 2 mL H<sub>2</sub>O followed by centrifugation (30,000 x g for 25 min.) Crude lysate was dialyzed against buffer A. Crude lysate was then passed through a DEAE fast flow column (2.5 x 13 cm) equilibrated with buffer A. Column was washed with buffer A and protein eluted using a linear NaCl gradient (25-400 mM). Fractions containing the protein were pooled and placed into dialysis against buffer B (25 mM potassium phosphate, pH 6.9), and then dialyzed against buffer C (25 mM potassium phosphate, pH 6.8). Protein was then passed through an HA column (1.5 x 16 cm) equilibrated with buffer C. Protein was isocratically eluted with buffer C and dialyzed against the first demetalation buffer, buffer D (25 mM Hepes pH 7.5, 20 mM NaCl, 500 $\mu$ M EDTA, 3 g chelex resin), followed by dialysis in buffer E (25 mM TMA-Hepes, pH 7.5). Protein was concentrated using a nitrogen pressure cell and an Amicon 10K molecular weight cut-off membrane. Protein was aliquoted, flash-frozen on dry ice, and stored at -80°C.

### *Activity Assays for Mutant Protein*

In a typical reaction, 5  $\mu$ M enzyme was allowed to equilibrate with 100  $\mu$ M Mn(II) and 200 mM GSH in 25 mM Hepes, pH 7.5. The reactions were initiated by the addition of 25 mM fosfomycin and allowed to proceed for several minutes to an hour. Reactions



were quenched by the addition of 50  $\mu\text{L}$   $\text{CHCl}_3$  and vigorous vortexing, followed by immediate freezing on dry ice. Reactions thawed and centrifuged to pellet precipitated protein. The aqueous layer was removed and demetalated with chelex resin for 3 hours. Chelex resin was pelleted and the remaining aqueous layer was used for NMR analysis after the addition of  $\text{D}_2\text{O}$ .

## CHAPTER III

### PURIFICATION AND PRELIMINARY CHARACTERIZATION OF THE FOSX ENCODED IN THE GENOME OF *BRUCELLA MELITENSIS*

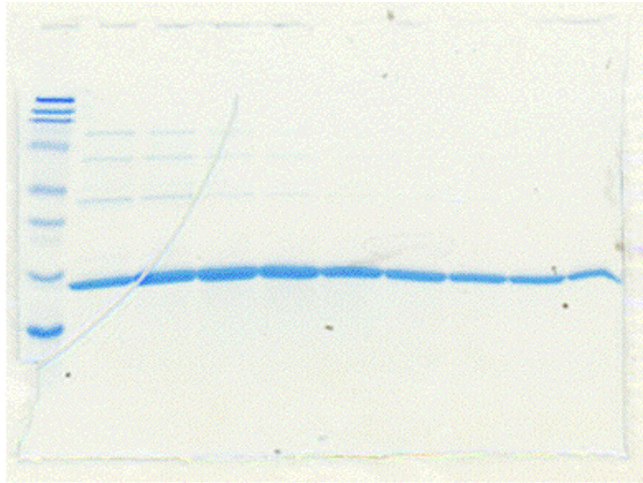
#### Results

##### *Expression, Purification, and ESI-Mass Spectrometry of B. melitensis FosX*

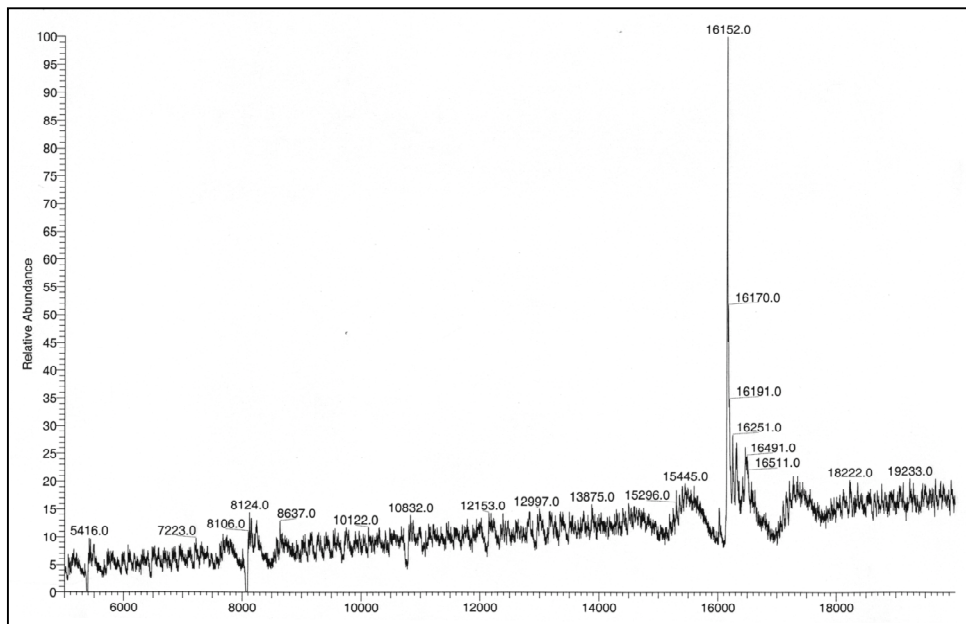
Expression and purification of the *B. melitensis* FosX protein yielded 15 mg of pure protein per liter of cell culture (Figure 11a). The calculated molecular weight of the protein is 16149 Da, which agrees with the molecular weight observed from SDS-PAGE (protein observed just below the standard marker lysozyme, 20,461 Da, and above aprotinin, 7,100 Da) and ESI-mass spectrometry (16152 Da) (Figure 11b).

##### *Determination of Metal Preference by <sup>31</sup>P NMR Spectroscopy*

Activity of the *B. melitensis* FosX was monitored in the presence of different divalent metal cations:  $Mn^{2+}$ ,  $Cu^{2+}$ ,  $Co^{2+}$ ,  $Mg^{2+}$ ,  $Zn^{2+}$ ,  $Ni^{2+}$ , and  $Fe^{2+}$ . Conversion of fosfomycin into diol product was observed by <sup>31</sup>P NMR (Figure 12). In the presence of 300 nM enzyme, 25 mM fosfomycin, and 100  $\mu$ M  $Cu^{2+}$ , 42% product conversion was observed after 20 minutes, the highest conversion observed under these conditions. The metal preference of the *B. melitensis* FosX, as judged by percent product conversion under a standard set of conditions, was  $Cu^{2+} > Mn^{2+} > Co^{2+} > Ni^{2+} > Zn^{2+} > Mg^{2+} \approx Fe^{2+}$ .



a



b

**Figure 11.** Purification of *B. melitensis* FosX yields pure protein of the correct molecular weight. (a) SDS-PAGE of fractions collected from the HA purification column (b) ESI-MS of purified *B. melitensis* FosX protein.

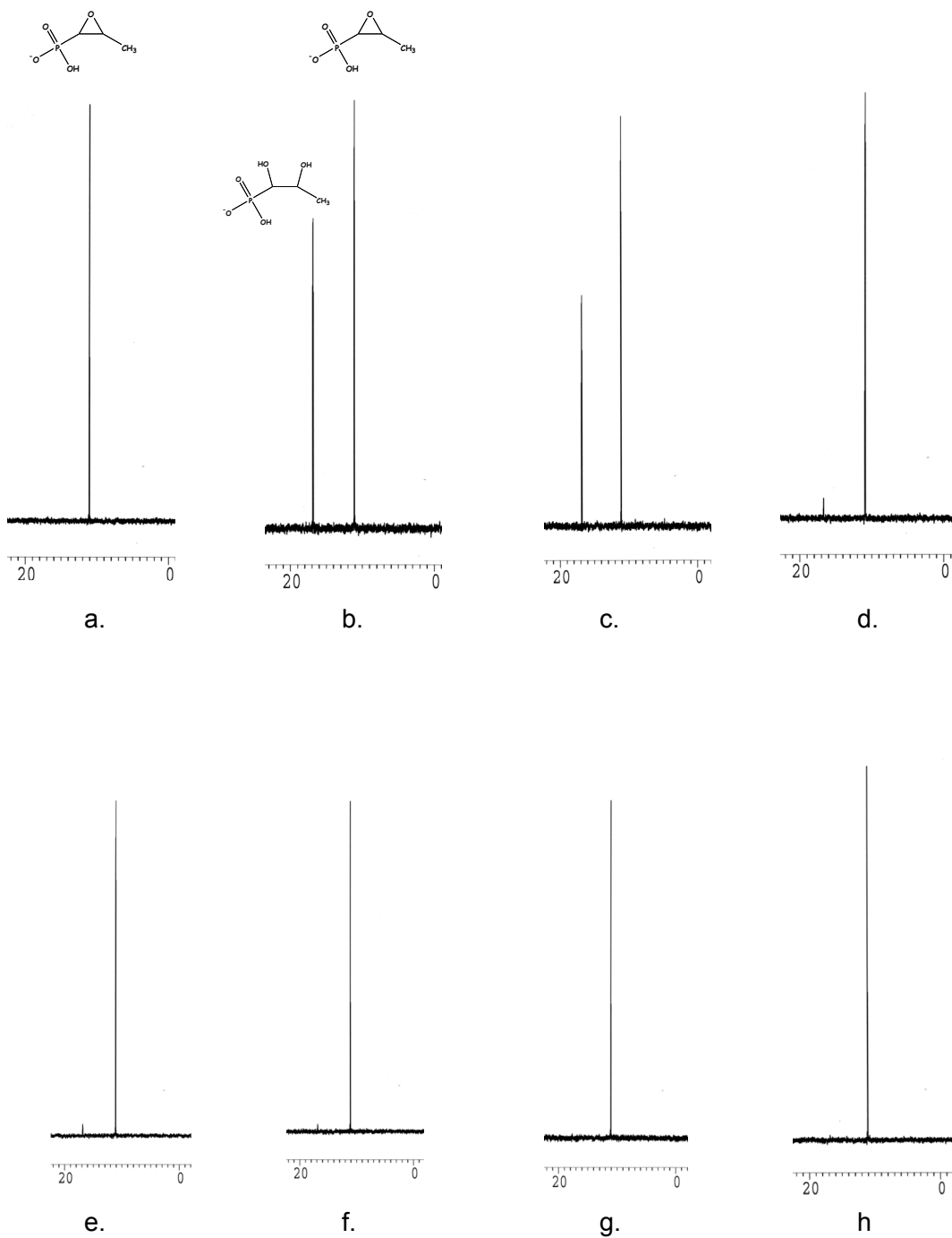


**Figure 12.** Catalytic activity of the *B. melitensis* FosX in the presence of various divalent metal cations: (a) no metal, (b)  $\text{Cu}^{2+}$ , (c)  $\text{Mn}^{2+}$ , (d)  $\text{Co}^{2+}$ , (e)  $\text{Ni}^{2+}$ , (f)  $\text{Zn}^{2+}$ , (g)  $\text{Mg}^{2+}$ , (h)  $\text{Fe}^{2+}$

### Estimation of the Turnover Number by $^{31}\text{P}$ NMR Spectroscopy

The turnover number for the *B. melitensis* FosX was estimated by looking at the  $^{31}\text{P}$  NMR spectra of reaction mixtures that yielded 10-15% product conversion (Figure 13). Using the peak heights and amount of product formed, the  $k_{\text{cat}}$  (in the presence of  $\text{Cu}^{2+}$ ) was estimated to be  $36 \text{ s}^{-1}$ .

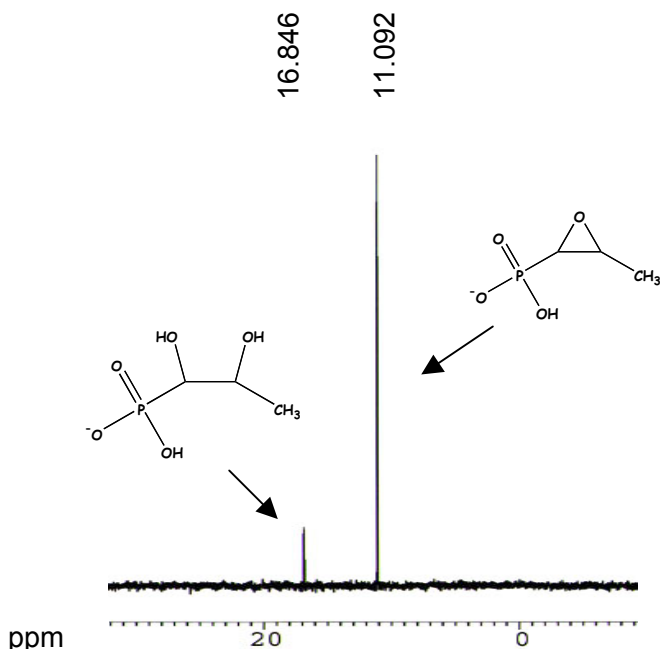
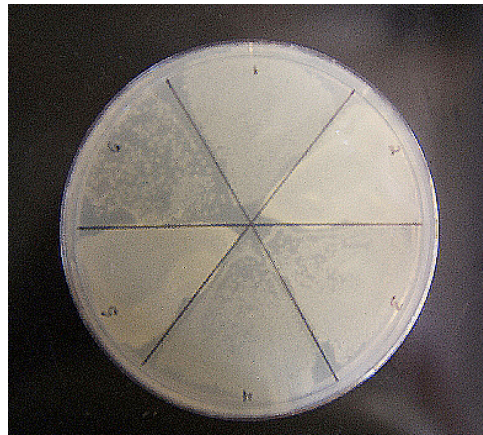


**Figure 13.**  $^{31}\text{P}$  NMR spectrum of a reaction mixture showing approximately 10% conversion of substrate into product.

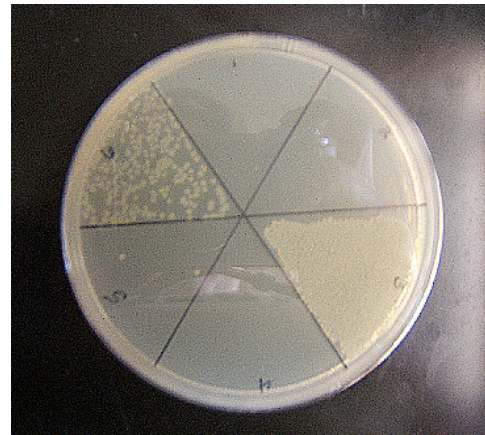
### Determination of the Minimum Inhibitory Concentration (MIC) of Fosfomycin

The expression plasmids encoding the FosX enzymes from *L. monocytogenes*, *B. melitensis*, *C. botulinum*, and *M. luti* were transformed into *E. coli* cells and grown on LB-agarose plates containing varying amounts of fosfomycin (0.0 mg/mL to 5.0 mg/mL). The minimum amount of fosfomycin at which inhibition of bacterial growth was observed by visual inspection was recorded as the MIC value for the enzyme, where a higher MIC

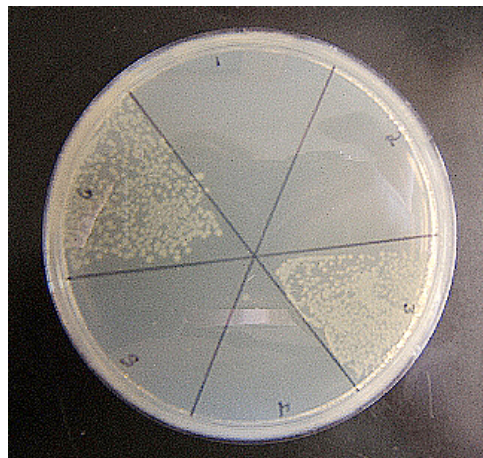
value indicates greater resistance. *P. aeruginosa* FosA and the empty expression vector were used as controls.



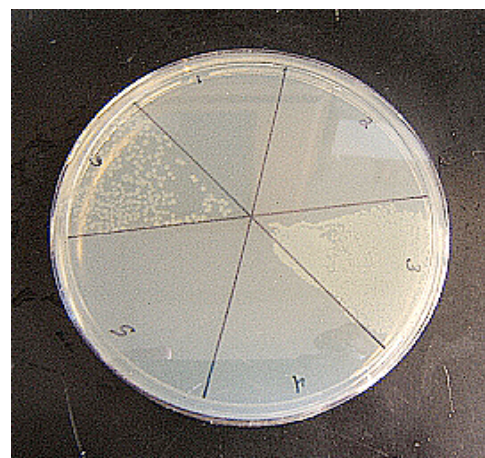
0 mg/mL Fosfomycin



0.025 mg/mL Fosfomycin



0.1 mg/mL Fosfomycin



5 mg/mL Fosfomycin

**Figure 14.** Bacterial growth and resistance on LB plates containing fosfomycin. BL21 *E. coli* cells were transformed with expression plasmids containing the FosX genes. Each plate was divided into six sections of bacterial growth (clockwise from top): 1= empty expression vector, 2 = *B. melitensis* FosX, 3 = *L. monocytogenes* FosX, 4 = *M. loti* FosX, 5 = *C. botulinum* FosX, and 6 = PA1129 FosA.

The only bacterial growth observed above 0.025 mg/mL fosfomycin was from cells transformed with *L. monocytogenes* FosX and *P. aeruginosa* FosA (PA1129). The results are summarized in Table 6.

**Table 6.** Summary of Results for MIC Experiments

Expression Plasmid	MIC
Empty vector	< 0.025 mg/mL
<i>L. monocytogenes</i> FosX	5 mg/mL
<i>B. melitensis</i> FosX	< 0.025 mg/mL
<i>M. loti</i> FosX	< 0.025 mg/mL
<i>C. botulinum</i> FosX	< 0.025 mg/mL
PA1129 FosA	5 mg/mL

To insure that the *B. melitensis* FosX was being expressed in the MIC assays, the *B. melitensis* FosX plasmid was transformed in Tuner (DE3) *E. coli* cells so that expression could be tightly regulated. Cultures were induced with 25  $\mu$ M IPTG for one hour prior to being streaked on the fosfomycin-containing plates. There was a slight increase in growth observed, raising the MIC value of *B. melitensis* FosX to 0.025 mg/mL (Figure 15). In terms of resistance, however, this increase was insignificant.

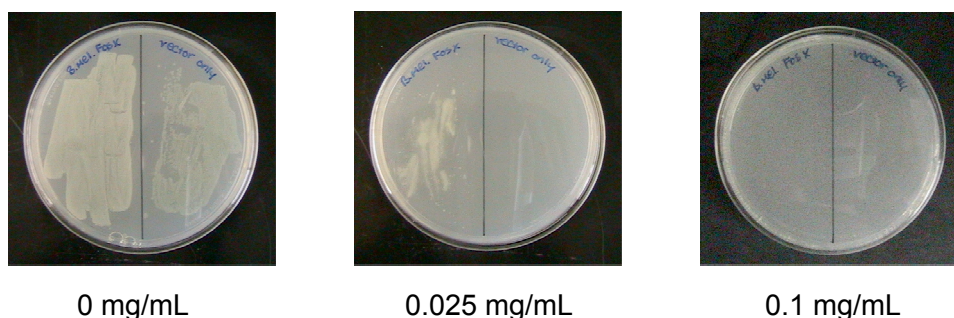


**Figure 15.** Induction of protein expression does not significantly alter the MIC value for *B. melitensis* FosX. Tuner cells containing either *B. melitensis* FosX expression vector or the empty vector were induced with IPTG to induce protein expression, and then plated on fosfomycin-containing plates.

Since it was known from previous experiments that the *B. melitensis* FosX shows preference for  $\text{Cu}^{2+}$  instead of  $\text{Mn}^{2+}$ , *E. coli* cells transformed with the *B. melitensis* FosX expression vector were cultured in media containing 200  $\mu\text{M}$   $\text{CuCl}_2$  prior to being plated on agarose plates containing varying amounts of fosfomycin. The MIC value did not change in this experiment (Figure 16).

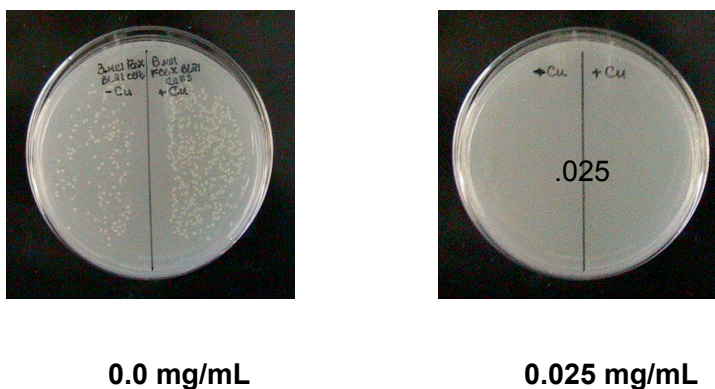


**Figure 16.** Cells transformed with the *B. melitensis* FosX expression vector and grown in the presence of copper do not have increased MIC values. The left sides of the plates contain cells grown without the addition of copper, and the right sides of the plates contain cells grown with the addition of exogenous copper.

### *X-ray Crystallography*

Although initial attempts to crystallize the *B. melitensis* FosX protein in the presence of copper were successful (Figure 17), preliminary screening revealed that the X-ray diffraction pattern was only to about 3 or 4 Å resolution and displayed diffuse scattering patterns. Attempts to optimize crystallization conditions did not improve the quality or resolution of the X-ray diffraction data.



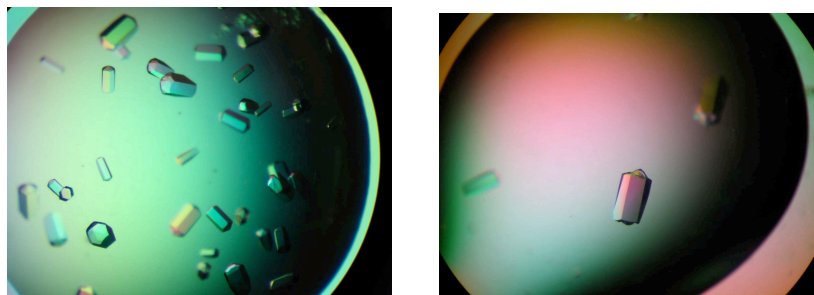


**Figure 17.** Protein crystals of *B. melitensis* FosX

### Discussion

After the initial discovery of enzyme-mediated inactivation of fosfomycin by fosfomycin resistance proteins, homologues of genomically encoded FosA proteins were found in a variety of bacteria. These homologues were later divided into classes designated FosA, FosB and FosX. Investigation of FosA protein activity revealed that these proteins were GSH transferases and all shared a  $Mn^{2+}$  dependency and were activated by the presence of  $K^+$ . Likewise, the FosB enzymes were also thiol-transferases, but utilized L-cysteine as a co-substrate instead of GSH. All members of the FosB class shared a dependency on  $Mg^{2+}$ . The more distantly related FosX proteins, however, were unique in that no thiol was involved in the reaction mechanism and instead, these enzymes were found to be expoxide hydrolases. Initial examination revealed that the members of FosX required  $Mn^{2+}$  for activity. Therefore, it was very surprising that the *B. melitensis* FosX was observed to prefer  $Cu^{2+}$  instead of  $Mn^{2+}$ . This unique metal preference was also observed for the *C. botulinum* FosX. Even more intriguing was the observation that these two enzymes with a different metal preference could proficiently catalyze the hydrolysis of fosfomycin *in vitro*, but could not confer resistance to fosfomycin in the biological context of *E. coli*. The turnover number of *B.*

*melitensis* FosX was estimated to be  $36 \text{ s}^{-1}$ , which is identical to the turnover number of the *L. monocytogenes* FosX—the FosX that confers robust resistance when expressed in *E. coli* and in the native organism as well. It appeared that this discrepancy of catalytic ability of the *B. melitensis* FosX might be explained by the different metal preference of this enzyme. To determine if this was the case, a more detailed analysis of metal binding was carried out and discussed in the following chapter.

## CHAPTER IV

### INVESTIGATION OF METAL BINDING KINETICS FOR THE FOSX PROTEINS

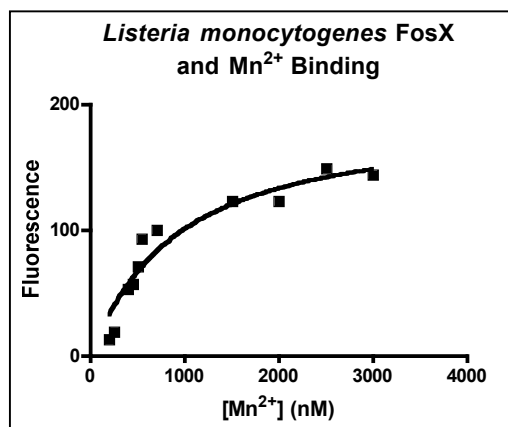
#### Results

##### *Steady State Metal Binding Analysis*

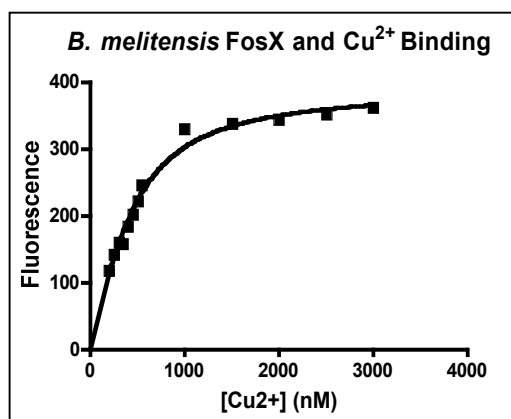
In order to determine equilibrium dissociation constants for metal binding to FosX proteins, the intrinsic protein fluorescence was exploited. Upon titration of 100  $\mu\text{M}$  FosX protein with metal, changes in fluorescence were observed and plotted as a function of metal concentration. The data were fit with the bound verses total equation, which takes into the account that binding is tight, and hence  $K_D$  is small. This equation takes into consideration that most of the protein is in the protein-metal complex since the concentration of protein is approximately equal to  $K_D$ :

$$Y = \frac{-(-1(K_d + X + \text{Cap})) + \sqrt{((K_d + X + \text{Cap})^2 - (4 X \text{Cap}))}}{2} \quad (\text{equation 1})$$

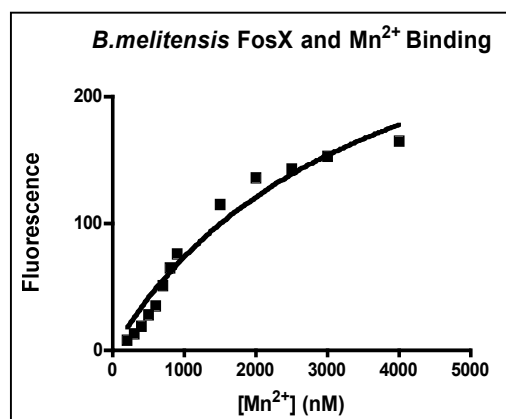
where  $\text{Cap} = [E_{\text{total}}] \cdot [M^{2+}_{\text{total}}]$ . Plots of the experimental data are shown below (Figure 18).



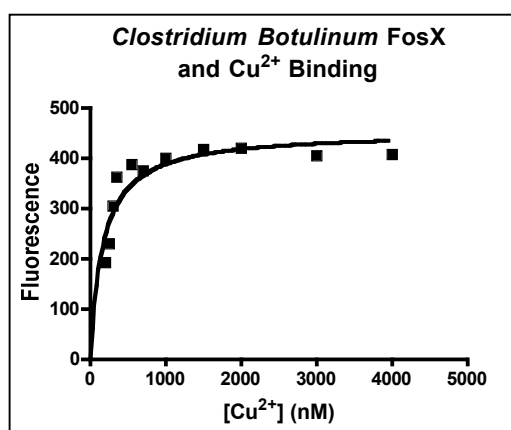
a



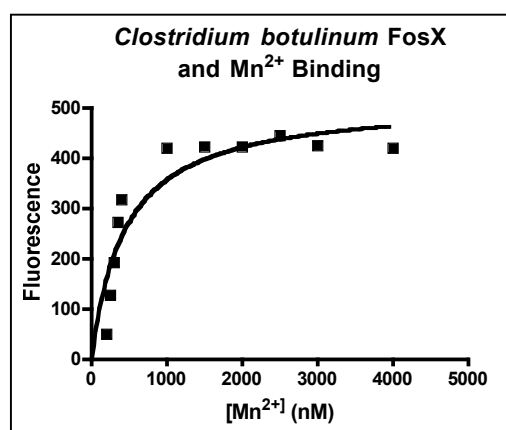
b



c



d



e

**Figure 18.** Steady state analysis of metal binding to the FosX proteins: relative change in intrinsic protein fluorescence at 335 nm upon metal titration of (a) *L. monocytogenes* FosX, (b, c) *B. melitensis* FosX, (d, e) *C. botulinum* FosX.

From the steady state data, it was evident that the *B. melitensis* FosX and *C. botulinum* FosX, the proteins suspected to utilize Cu<sup>2+</sup> for activity, demonstrate tighter binding of Cu<sup>2+</sup> than of Mn<sup>2+</sup>. In fact, binding of Cu<sup>2+</sup> to these enzymes appeared to be tighter than that of Mn<sup>2+</sup> binding to the *L. monocytogenes* FosX (Table 7).

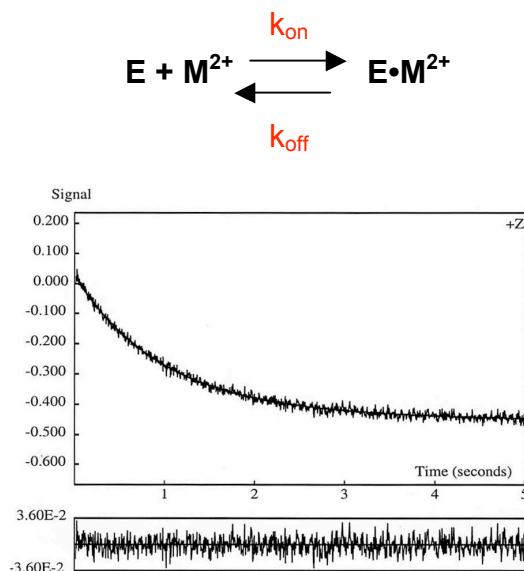
**Table 7.** Equilibrium Dissociation Constants for Metal Binding to FosX Proteins.

FosX Enzyme	Metal	K <sub>D</sub> (nM)
<i>L. monocytogenes</i>	Mn <sup>2+</sup>	789 ± 222
<i>B. melitensis</i>	Cu <sup>2+</sup>	214 ± 20
<i>B. melitensis</i>	Mn <sup>2+</sup>	3184 ± 925
<i>C. botulinum</i>	Cu <sup>2+</sup>	166 ± 39
<i>C. botulinum</i>	Mn <sup>2+</sup>	444 ± 137

#### *Transient state metal binding analysis*

In order to study metal binding in more detail, stopped-flow spectroscopy was used to make transient state kinetic measurements. These experiments utilized rapid mixing of 200 nM enzyme and varying concentrations of metal (1.2 μM to 180 μM) so that changes in intrinsic protein fluorescence could be measured on a millisecond time scale. Using this experimental design, on and off rate constants for metal binding were determined, allowing for the calculation of an apparent equilibrium dissociation constant (Figure 19). Plotting the observed rate constant as a function of metal concentration yields a linear relationship where the slope equals k<sub>on</sub> and the y-intercept equals k<sub>off</sub>. Unfortunately, extrapolation of the data was sometimes too close to zero to obtain an

accurate off rate constant of binding. In addition, the Prizm software used to analyze the data did not always result in a good fit of the data.



$$k_{\text{obs}} = k_{\text{off}} + k_{\text{on}} [M^{2+}]$$

$$K_{\text{D (app)}} = k_{\text{off}}/k_{\text{on}}$$

**Figure 19.** Diagram showing a typical change in fluorescence and illustrating the stopped-flow experimental design used to determine  $k_{\text{on}}$  and  $k_{\text{off}}$  and the apparent equilibrium dissociation constant.

When the *B. melitensis* FosX protein was rapidly mixed with  $\text{Cu}^{2+}$  in the stopped-flow, the observed change in intrinsic protein fluorescence was fit to a double exponential, yielding two distinct observed rate constants. This implies that metal binding is a two step process. From the rate 1 data, it was observed that the on rate constant for metal binding was very fast, and the off rate constant relatively slow, giving an apparent dissociation constant in the low nanomolar range, thus indicating tight binding (Figure 20). Analysis of rate 2 data was more difficult (Figure 20). Data were fit

to a hyperbola in this case, however it was unclear what information this reveals about metal binding except for the fact that it is a two step process.

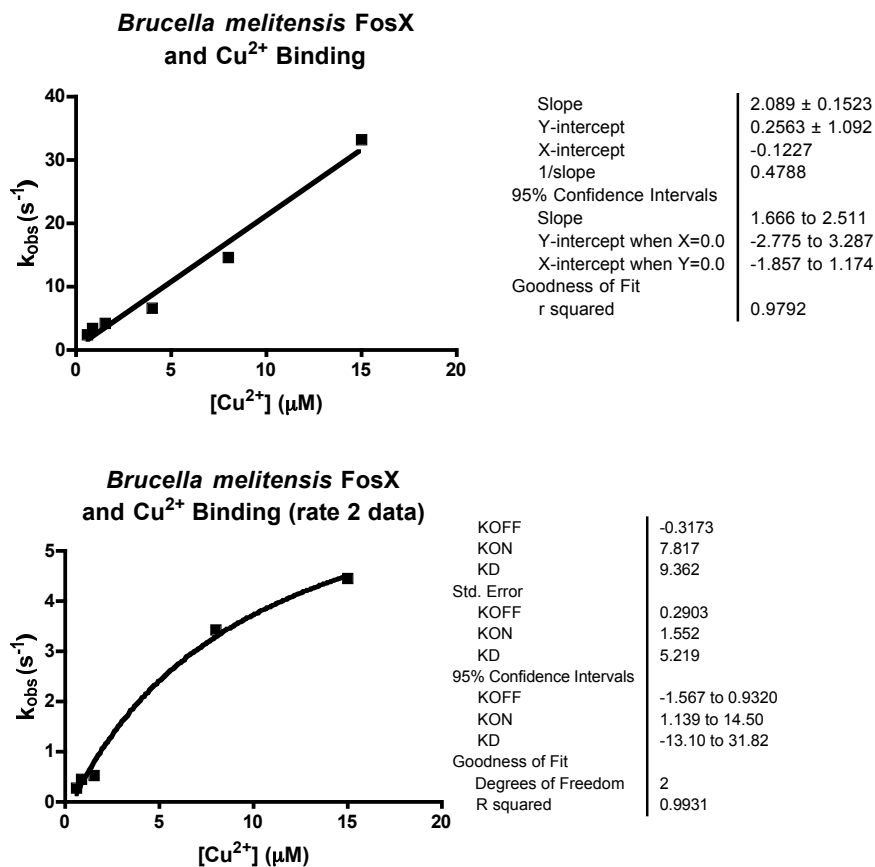


**Figure 20.** Stopped flow analysis of Cu<sup>2+</sup> binding to *B. melitensis* FosX reveals a two step process. The top plot is of the rate 1 data and the bottom plot is for rate 2 data.

Binding of  $Mn^{2+}$  to *B. melitensis* FosX revealed a much slower on rate constant with approximately the same off rate constant, yielding an apparent dissociation constant this time in the low micromolar range. As with  $Cu^{2+}$  binding, this experiment revealed a two step process for metal binding (Figure 21).

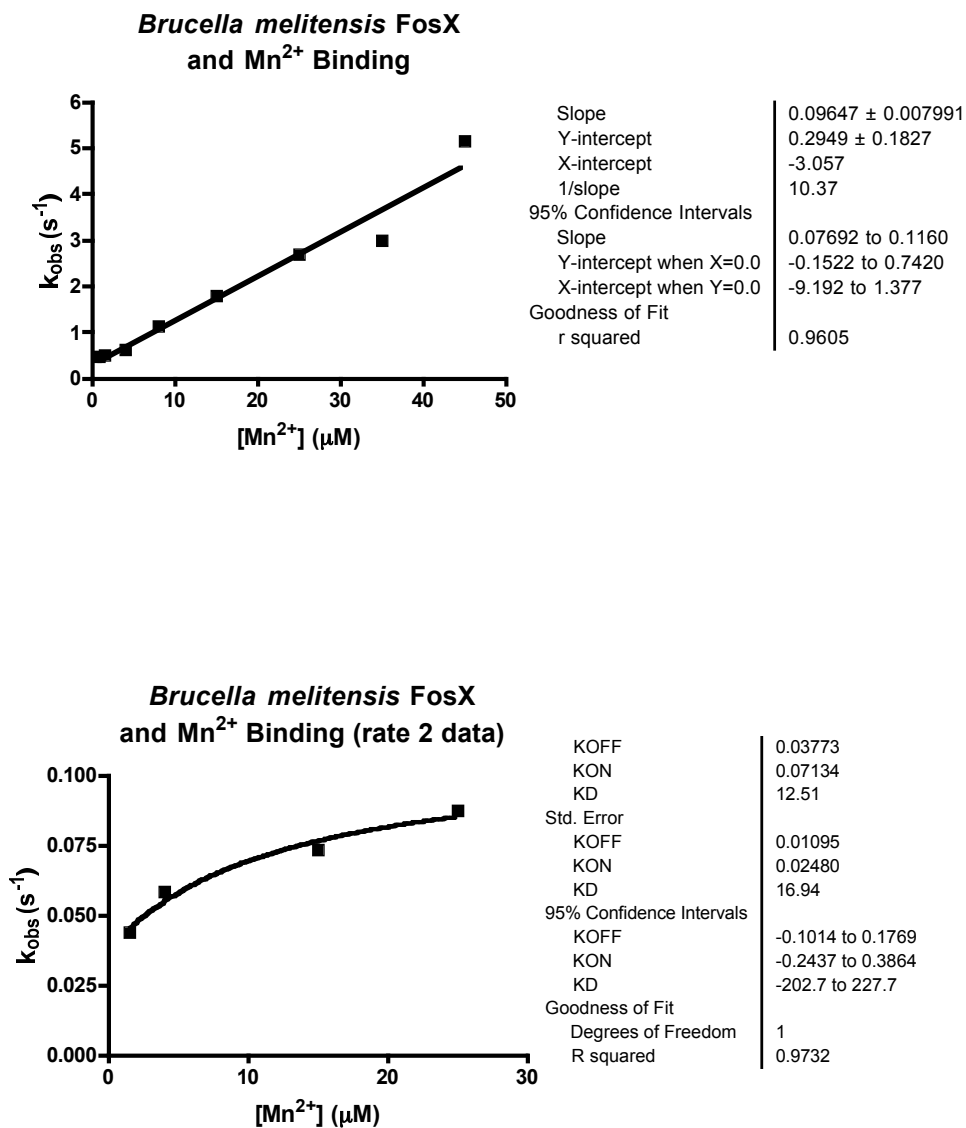


**Figure 21.** Stopped flow analysis of  $Mn^{2+}$  binding to *B. melitensis* FosX reveals a two step process.



As with the *B. melitensis* FosX, analysis of *C. botulinum* FosX and  $\text{Cu}^{2+}$  binding revealed a fast on rate constant of binding. The linear regression, however, did not allow for determination of the off rate constant in this case, since the off rate constant is probably in actuality very close to zero. In this case, the off rate constant was determined by an alternative method, which will be described later in this chapter. As with previous stopped-flow experiments, a two step process for metal binding was observed (Figure 22).

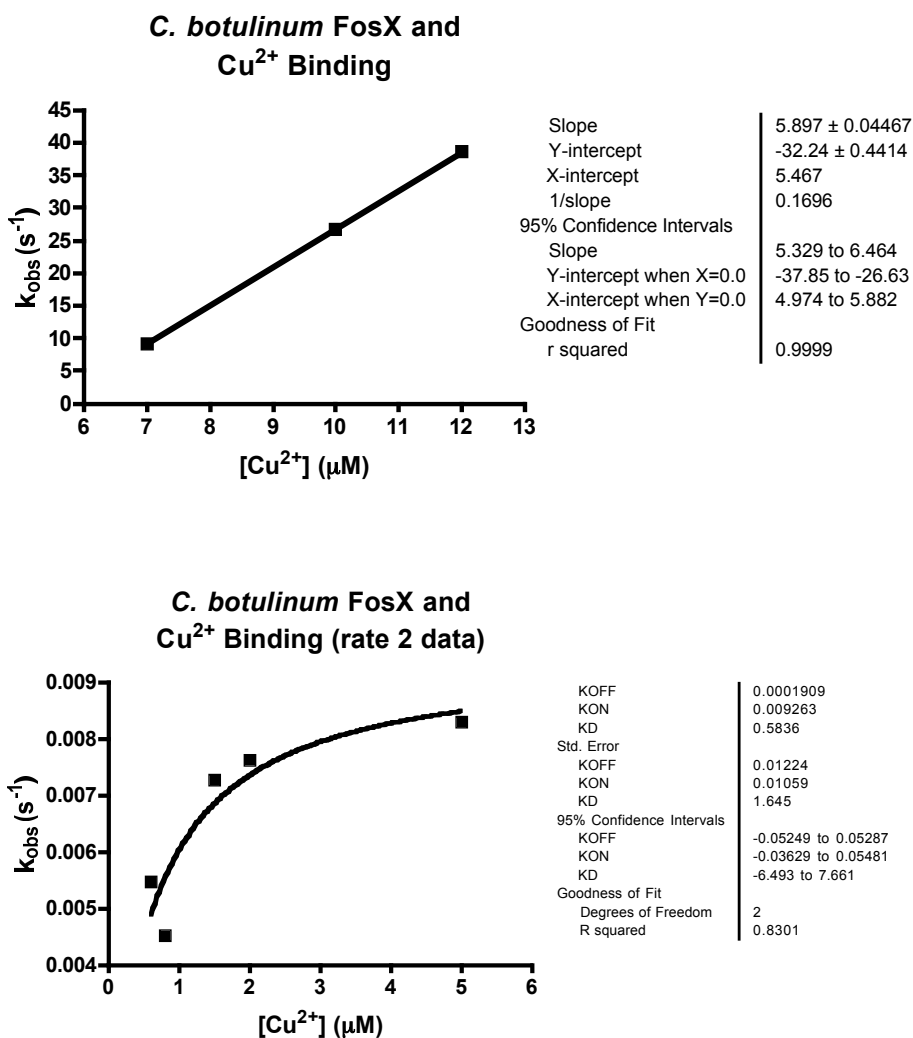


**Figure 22.** Stopped flow analysis of  $\text{Cu}^{2+}$  binding to *C. botulinum* FosX reveals a two step process.

*C. botulinum* FosX binding to  $Mn^{2+}$  demonstrated a much slower on rate constant, which was to be expected since it was believed that this enzyme prefers  $Cu^{2+}$ .

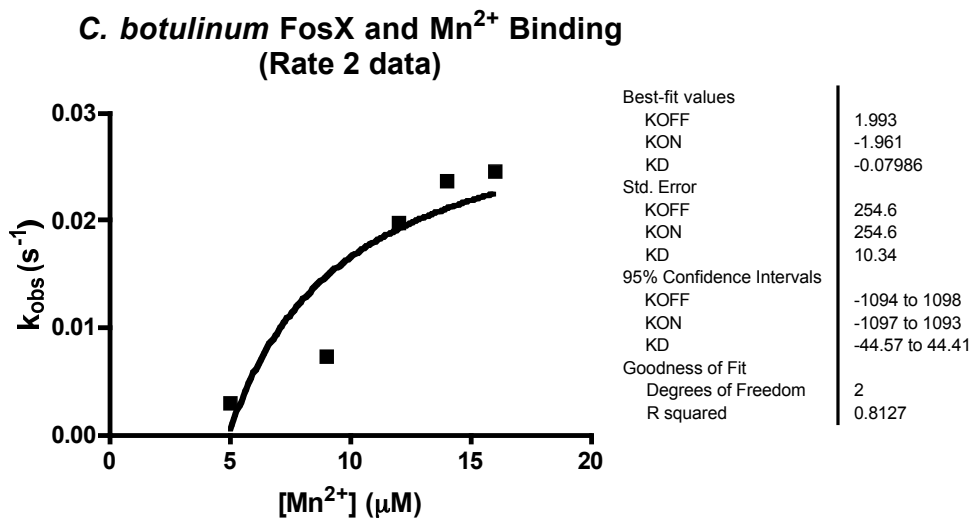
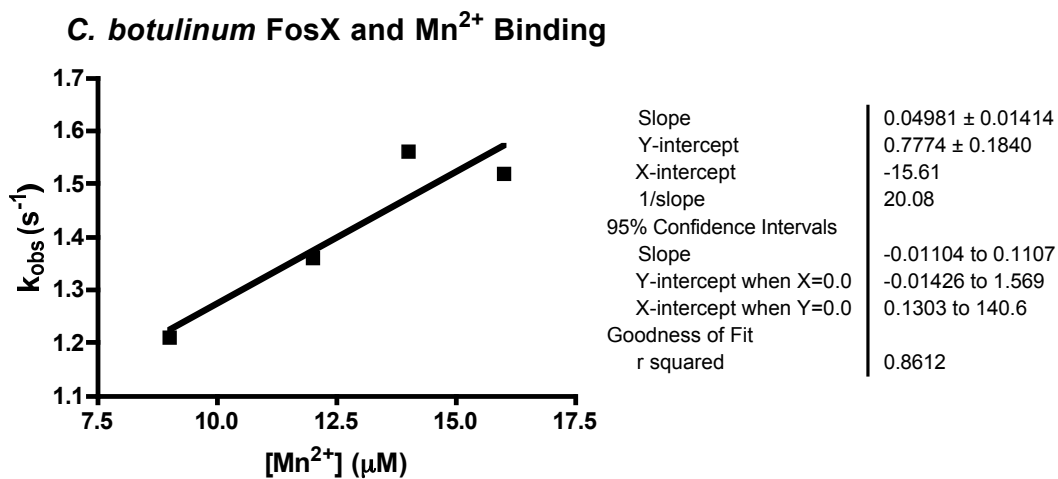


**Figure 23.** Stopped flow analysis of  $Mn^{2+}$  binding to *C. botulinum* FosX reveals a two step process.

Analysis of *L. monocytogenes* binding to  $Mn^{2+}$  revealed a two step binding process as well, with a relatively slow off-rate constant, giving an apparent dissociation constant in the nanomolar range.

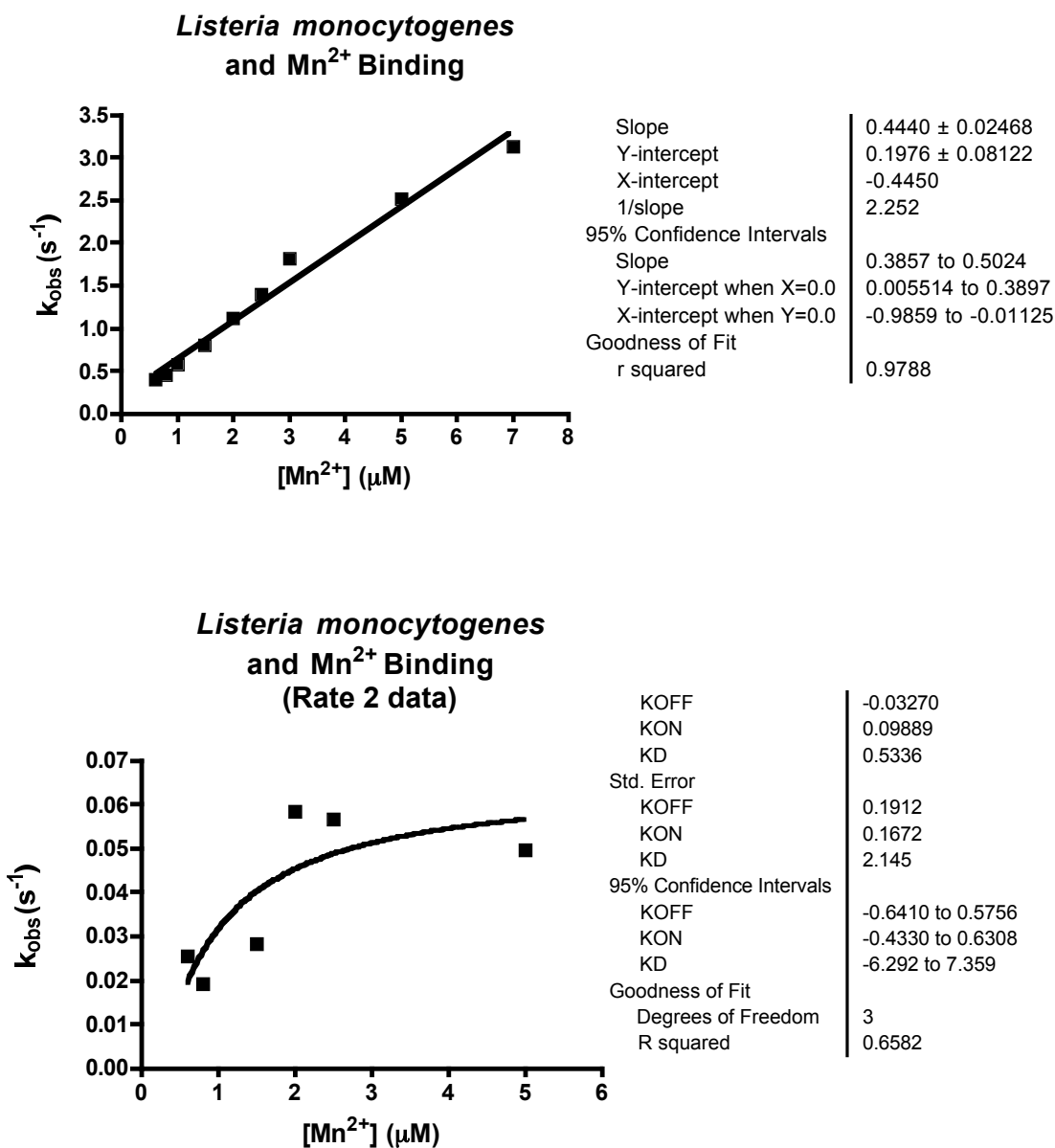


**Figure 24.** Stopped flow analysis of  $Mn^{2+}$  binding to *L. monocytogenes* FosX reveals a two step process.

Although the stopped-flow data supplied us with much information, in most cases, the off rate constant for metal binding was unreliable since the y-intercept of the linear regression was too close to zero. To observe off rate constants directly so that a more accurate dissociation constant could be determined, the experiment illustrated in Figure 25 was used.

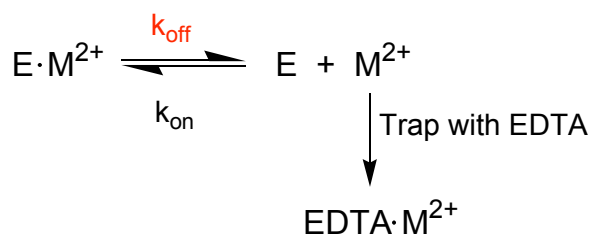


**Figure 25.** Diagram illustrating the stopped-flow experimental design used to observe  $k_{off}$  directly.

This experiment utilized an excess of EDTA (25 mM) to trap the metal so that off rate constants could be directly observed using stopped-flow instrumentation (Figure 26). From the data, it was evident that the off rate for  $Mn^{2+}$  from *L. monocytogenes* FosX is extremely slow, as would be anticipated for an enzyme that binds a metal so tightly. The *B. melitensis* FosX and *C. botulinum* FosX have relatively slow off rates for  $Cu^{2+}$  binding, while the off rate for  $Mn^{2+}$  binding to *C. botulinum* is relatively fast (Table 8).

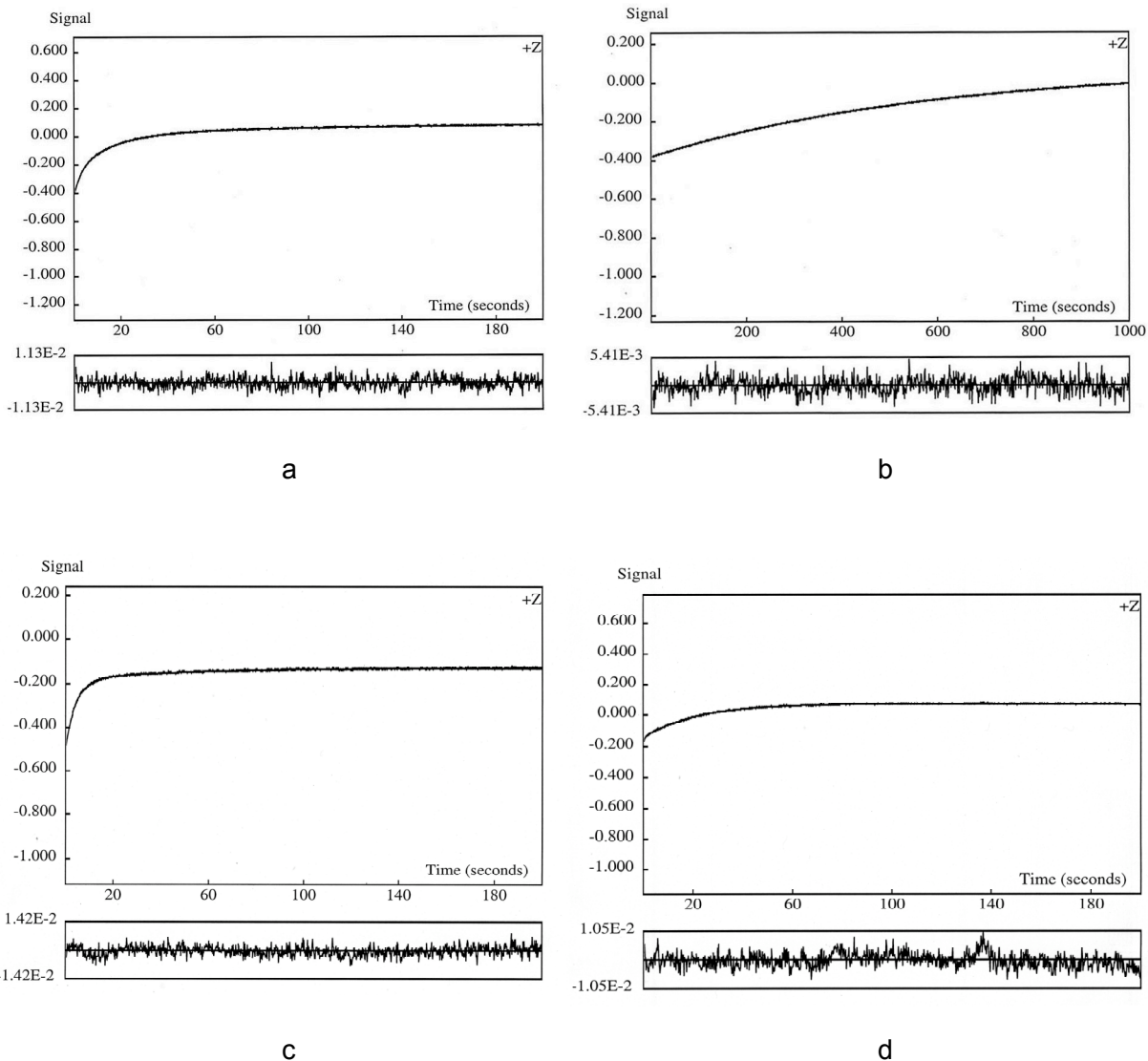


**Figure 26.** Stopped-flow data traces observed upon rapid mixing of the enzyme-metal complex with EDTA (a)  $\text{Cu}^{2+}$  and *B. melitensis* FosX (b)  $\text{Mn}^{2+}$  and *L. monocytogenes* FosX (c)  $\text{Cu}^{2+}$  and *C. botulinum* FosX (d)  $\text{Mn}^{2+}$  and *C. botulinum* FosX.

**Table 8.** Observed Off Rate Constants for Metal Binding

FosX Enzyme	Metal	Observed $k_{\text{off}}$ ( $\text{s}^{-1}$ )
<i>L. monocytogenes</i>	$\text{Mn}^{2+}$	$0.00168 \pm 0.00007$
<i>B. melitensis</i>	$\text{Cu}^{2+}$	$0.372 \pm 0.001$
<i>B. melitensis</i>	$\text{Mn}^{2+}$	n.d.
<i>C. botulinum</i>	$\text{Cu}^{2+}$	$0.233 \pm 0.002$
<i>C. botulinum</i>	$\text{Mn}^{2+}$	$1.80 \pm 0.14$

n.d. = not determined

Overall, the steady state metal binding data agrees well with the data from the transient state experiments. From the data, it is apparent that the *B. melitensis* and *C. botulinum* FosX proteins demonstrate a preference for  $\text{Cu}^{2+}$  due to their low dissociation constants and reasonably slow off rates of  $\text{Cu}^{2+}$  binding, in addition to displaying higher catalytic activity in the presence of  $\text{Cu}^{2+}$ . (Table 8). Therefore, it would be reasonable to expect that Cu is indeed the metal utilized by these enzymes in their native organisms.

**Table 9.** Summary of Metal Binding Dissociation Constants for the FosX Proteins

FosX Enzyme	Metal	$K_D$ (steady-state) (nM)	$K_D$ (presteady-state) (nM)	Observed $k_{\text{off}}$ ( $\text{s}^{-1}$ )	$K_D$ (from observed $k_{\text{off}}$ ) (nM)
<i>L. monocytogenes</i>	$\text{Mn}^{2+}$	$789 \pm 222$	$445.0 \pm 0.41$	$0.00168 \pm 0.00007$	$4.0 \pm 0.04$
<i>B. melitensis</i>	$\text{Cu}^{2+}$	$214 \pm 20.4$	$122 \pm 4.3$	$0.372 \pm 0.001$	$178 \pm 2.7$
<i>B. melitensis</i>	$\text{Mn}^{2+}$	$3184 \pm 925$	$3056.9 \pm 0.63$	n.d.	n.d.
<i>C. botulinum</i>	$\text{Cu}^{2+}$	$166 \pm 39.1$	n.d.	$0.233 \pm 0.002$	$39.5 \pm 0.01$
<i>C. botulinum</i>	$\text{Mn}^{2+}$	$444 \pm 137$	$15607 \pm 0.4$	$1.8 \pm 0.1$	$36137 \pm 0.3$

n.d. = not determined

## Discussion

The data from the steady state and transient state binding studies agree well with the metal preferences first observed by  $^{31}\text{P}$  NMR for the FosX enzymes; unlike the  $\text{Mn}^{2+}$ -dependent *M. loti* and *L. monocytogenes* FosX enzymes, the FosX enzymes encoded by *B. melitensis* and *C. botulinum* demonstrate a preference for  $\text{Cu}^{2+}$  as their divalent metal cation. This is supported by their low equilibrium dissociation constants and slow off rates of Cu binding as compared to Mn. Although the transient state kinetic data revealed that metal binding is a two step process, the inability of the software to completely distinguish the second observed rate constant from the first observed rate constant led to inconsistent rate 2 data. Therefore, fitting rate 2 data was difficult and was unable to reveal the nature of the second step of the metal binding process. Since these proteins exist as dimers, however, one might speculate that a two step process is observed due to cooperativity of metal binding. However, in the case of cooperativity, the rate 2 data would be expected to yield a linear relationship, not a hyperbolic one as seen in the data above. Although not yet conclusive, it appears that the second step we are observing is not due to cooperativity but to some other conformational change of the enzyme-metal complex.

In addition, the data support metal preference as the explanation for the variable biological activity observed in *E. coli*. Research has suggested that bacteria maintain levels of Cu and Mn in the range of 10 to 100  $\mu\text{M}$ . However, the theory of a “free” metal pool in the case of Cu is beginning to seem impractical. Cu is one of the more toxic metals that a cell requires. The intracellular concentration must be controlled in order to prevent damage caused by this toxic, redox-active metal. Consequently, free forms of Cu are proposed to be too low in a cell to allow an apoprotein to obtain Cu. So how does an apoprotein obtain the necessary Cu cofactor? The answer lies in a system of

enzymes whose job is to control the amount and location of Cu within a cell. Intracellular metal trafficking systems are composed of copper transport ATPases and metal chaperones which are in charge of regulating, sequestering, and allocating Cu to the appropriate metalloenzymes (24). One of the best studied bacterial copper transport systems is the *Enterococcus hirae* system, which utilizes three proteins: the ATPase proteins CopA and CopB, and the copper chaperone CopZ (25).

Copper chaperones are small cytoplasmic proteins that are responsible for delivering Cu to Cu-dependent enzymes so that the free pool of available metal can be kept low in the cell. Interestingly, BLAST searches revealed a CopZ homolog in *Brucella melitensis* that is not present in *E. coli*. Further investigation revealed that since *E. coli* does not encode a true, stand-alone copper chaperone, it actually may generate a copper chaperone by proteolytic cleavage of its Cu-ATPase (26). Whatever the case, it is clear that there is large diversity when it comes to bacterial organization of the genes encoding the copper trafficking system, *i.e.* Cu-ATPase proteins and copper chaperones, giving rise to diversity in copper trafficking. If this is indeed the case, it may help explain why a Cu-dependent enzyme from *B. melitensis* may be unable to acquire the metal cofactor it needs in the biological setting of *E. coli*.

Taking this into consideration, it is apparent that metal preference of FosX proteins may play a role in the unexpected observations of the MIC assays. The Cu-dependent, catalytically proficient FosX enzymes from *B. melitensis* and *C. botulinum* may be unable to provide resistance in *E. coli* due to the unavailability of the necessary metal cofactor, not because they are inefficient at hydrolyzing fosfomycin in a biological setting. Although these enzymes can utilize  $Mn^{2+}$  *in vitro*, and there is likely to be a “free” pool of Mn in *E. coli*, the  $K_D$  values for  $Mn^{2+}$  binding to these proteins are most likely too high to allow for efficient acquisition of metal in *E. coli*, thus explaining the discrepancy observed between *in vitro* and *in vivo* catalytic ability.



Although true MIC values cannot be obtained using the MIC assays described in this work, it is reasonable to expect that the *B. melitensis* FosX is quite capable of providing the *B. melitensis* organism with resistance to fosfomycin, especially considering that this enzyme's *in vitro* activity is virtually the same as the *in vitro* activity of the biologically active *L. monocytogenes* FosX. Likewise, it is also reasonable that the *C. botulinum* FosX should provide some resistance to the *botulinum* organism even though it displays weaker catalytic activity *in vitro*. Although an attempt was made to supplement copper to growing *E. coli* cells in the MIC assays, it is not surprising that the copper transport and trafficking system in *E. coli* did not allow accumulation of this toxic metal to a concentration that would be adequate for metal acquisition by an apoprotein. To resolve this discrepancy, MIC assays would need to be performed in the native organism, which in the case of these two extremely pathogenic organisms, remains impossible in our current environment.

## CHAPTER V

### MUTAGENESIS OF THE CATALYTICALLY TEPID AND PROMISCUOUS FOSX FROM *MESORHIZOBIUM LOTI*

#### Results

##### *Creation of a K<sup>+</sup> Binding Loop in M. loti FosX*

In an attempt to enhance the promiscuous and catalytically poor FosA activity of the *M. loti* FosX, residues capable of forming a K<sup>+</sup> binding loop were inserted by mutation of existing residues. It is proposed that the ability to bind K<sup>+</sup> is important for FosA catalytic activity, and would therefore enhance the poor FosX activity of this enzyme and perhaps even its promiscuous FosA activity as well.

The residues comprising the K<sup>+</sup> binding loop in FosA were elucidated by structural observation and sequence alignments. The residues comprising the loop in *P. aeruginosa* FosA are underlined below (Figure 27).

<i>P. aeruginosa</i> FosA	<sup>87</sup> REWK <u>QNR</u> --- <u>SEGD</u> SFYFL <sup>102</sup>
Tn2921 FosA	TIWKQNK---SEGASFYFL
<i>M. loti</i> FosX	<sup>92</sup> DMRPPRPRVEGEGRSIYFY <sup>110</sup>
<i>L. monocytogenes</i> FosX	EMKPERPRVQGEGRSIYFY

**Figure 27.** Sequence Alignment of FosA K<sup>+</sup> Loop with FosX. The underlined residues represent those involved in interaction with K<sup>+</sup>.

This sequence alignment revealed that the corresponding residues in FosX contained an insertion of three residues and the region was overall dissimilar to FosA. In order to create a functional  $K^+$  binding loop analogous to the loop in FosA, the following mutations were made in the *M. luti* FosX DNA using the QuikChange method of site-directed mutagenesis:  $\Delta R99/\Delta V100/\Delta E101/P96Q/R97N/P98R/G102S$ . The same set of mutations were made in the E44G/F46Y/M57S mutant (active site mutations which yield a 250-fold enhancement of FosA activity) background as well. When the activity of these mutants was evaluated, no enhancement of FosX or FosA activity was observed in the presence of  $K^+$ . In fact, overall catalytic activity was actually decreased (Figures 28 and 29).

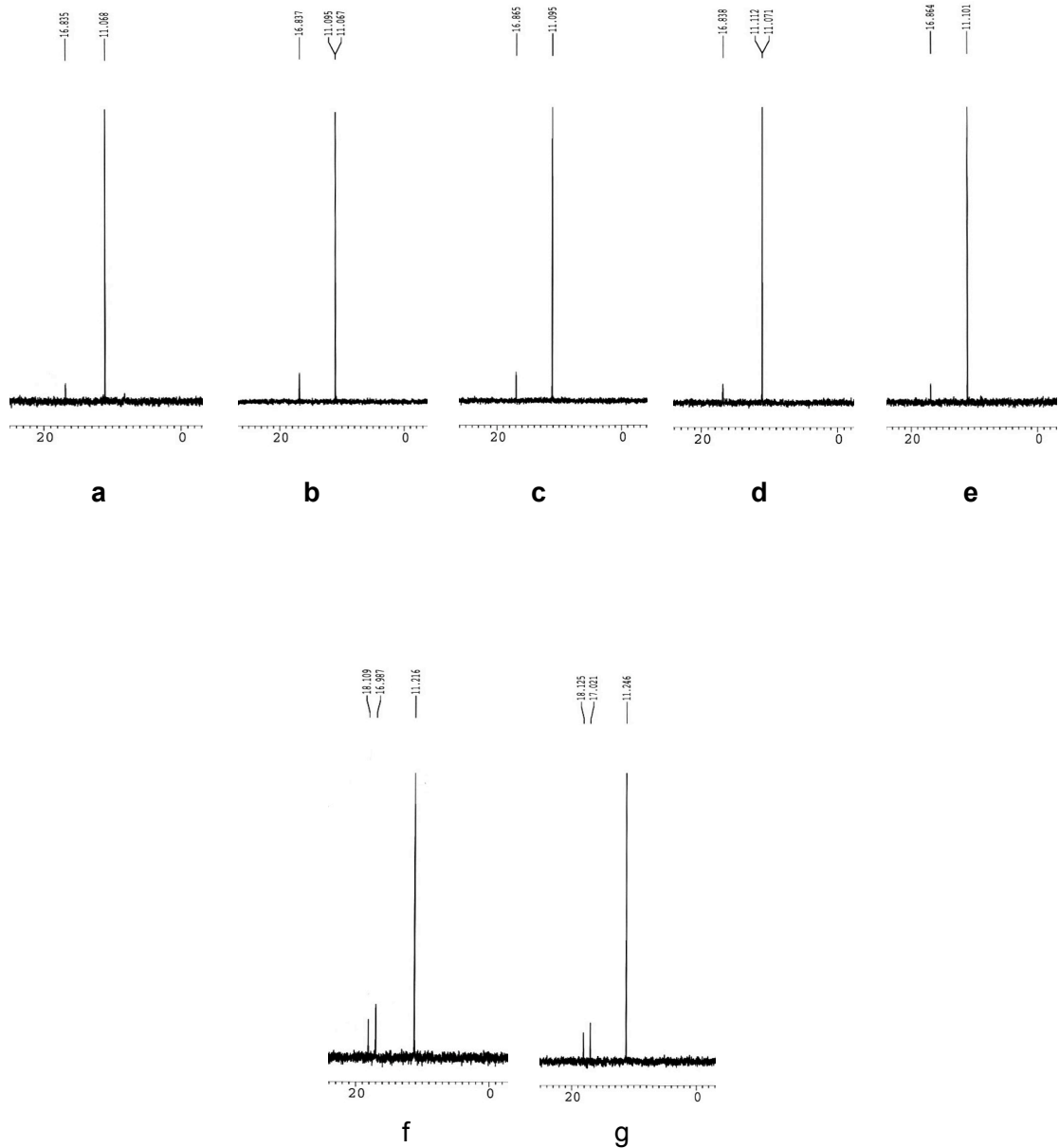


**Figure 28.** Activity of *M. loti* FosX containing mutations for a  $K^+$  binding loop. Fosfomycin is seen at 11.1 ppm, diol product is at 16.9 ppm and the FosA GSH-conjugated product is seen at 18.1 ppm. (a)  $^{31}P$  NMR spectrum of TMA-Fosfomycin, notice that TMA-fosfomycin contains a small amount of diol contaminant at 16.9 ppm which was subtracted from the other spectra in turnover calculations, (b) WT *M. loti* (c) WT *M. loti* plus  $K^+$  (d)  $K^+$  loop mutant, no  $K^+$  present, (e)  $K^+$  loop mutant, plus  $K^+$  (f)  $K^+$  loop mutant in presence of GSH, no  $K^+$  present, (g)  $K^+$  loop mutant in presence of GSH, plus  $K^+$

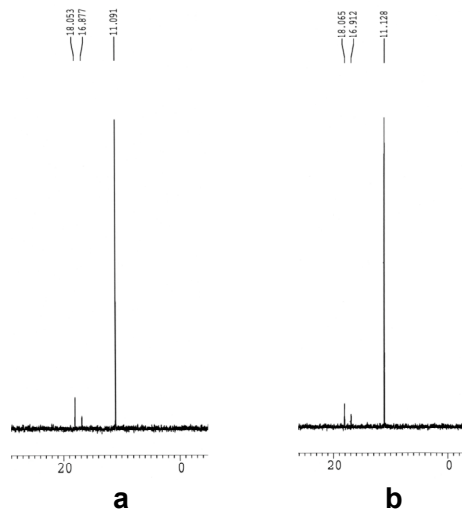


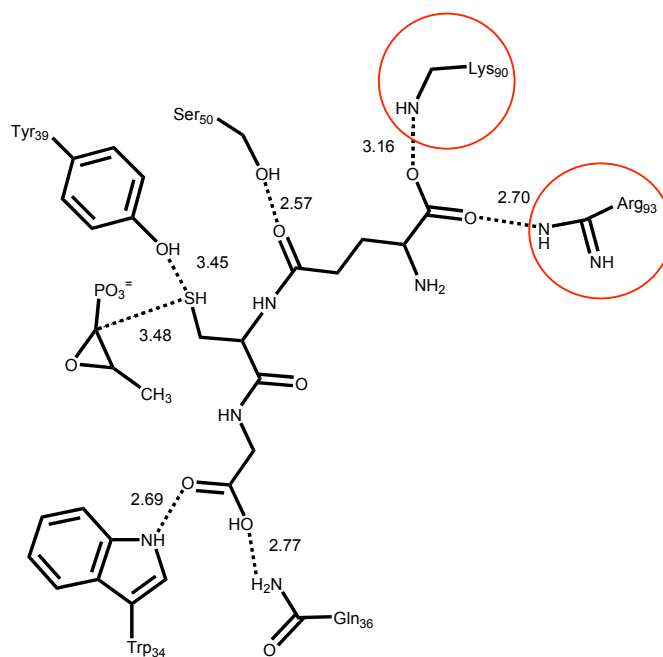
**Figure 29.** Activity of *M. loti* FosX containing the K<sup>+</sup> loop mutations and E44G/F46Y/M57S mutant background (a) without presence of K<sup>+</sup> (b) in presence of K<sup>+</sup>. As noted in Figure 28, the TMA-fosfomycin contains diol contaminant at 16.9 ppm.

A second attempt was made to create a functional K<sup>+</sup> binding loop in *M. loti* FosX. In addition to the mutations created previously, the following mutations were made as well: R94W/P95K/R105D. These mutants were made in the E44G/F46Y/M57S,  $\Delta$ R100/ $\Delta$ V101/ $\Delta$ E102/P97Q/R98N/P99R/G103S background. Unfortunately, this mutant did not demonstrate enhancement of activity in the presence of K<sup>+</sup> (Table 10).

In an alternative approach for enhancement of FosA activity, the *M. loti* FosX was mutated in an attempt to create a more favorable GSH binding site, which would consequently enhance the promiscuous FosA activity of this enzyme. This seemed to be the necessary next step since the E44G/F46Y/M57S mutant displayed a 250-fold increase in FosA activity but only at very high concentrations of GSH. By comparison of sequence alignments and computational work previously done with *P. aeruginosa* FosA (Figure 31), the following mutations were made: P95K/P98R in the E44G/F46Y/M57S mutant background.

*M. loti* FosX                   <sup>92</sup>D M R P P R P R V E G E G R S<sup>106</sup>  
*P. aeruginosa* FosA       <sup>87</sup>R E W **K** Q N **R** - - - S E G D S<sup>98</sup>

a.



b.

**Figure 30.** Sequence alignment and computational modeling reveal residues that need to be mutated in *M. loti* FosX to enhance GSH binding. (a) Sequence alignment of FosA and FosX around the proposed GSH binding site. (b) Computational docking of GSH onto FosA reveals residues proposed to interact with GSH. The two residues circled in red correspond to residues that were mutated into *M. loti* FosX to enhance GSH binding.

Unfortunately, the attempt to enhance GSH binding in *M. loti* FosX did not result in increased FosA activity of this enzyme. All of the mutagenesis data described above is summarized in Table 10.

**Table 10.** Summary of Catalytic Activity for the Different *M. loti* FosX Mutants

Mutation	$k_{cat}(\text{FosX})$ ( $\text{s}^{-1}$ )	$k_{cat}(\text{FosA})$ ( $\text{s}^{-1}$ )
WT*	0.15	0.06
E44G/F46Y/M57S*	n.a.	1.5
K <sup>+</sup> Loop (WT background)**	0.002	0.001
K <sup>+</sup> Loop/E44G/F46Y/M57S	n.a.	0.3
Additional K <sup>+</sup> Loop Mutations/E44G/F46Y/M57S***	n.a.	0.15
P95K/P98R in E44G/F46Y/M57S	n.a.	0.06

n.a. = no activity detected

\*Kerry Fillgrove, unpublished results

\*\* $\Delta\text{R99}/\Delta\text{V100}/\Delta\text{E101}/\text{P96Q}/\text{R97N}/\text{P98R}/\text{G102S}$

\*\*\* $\Delta\text{R99}/\Delta\text{V100}/\Delta\text{E101}/\text{P96Q}/\text{R97N}/\text{P98R}/\text{G102S}$  plus R94W/P95K/R105D

## Discussion

Previous mutagenesis experiments involving the *M. loti* FosX were successful in enhancing the weak, promiscuous GST activity of this enzyme (Fillgrove, unpublished data). The E44G/F46Y/M57S active site mutations virtually abolished the enzyme's FosX activity and increased its promiscuous FosA activity 250-fold. It was hoped that further mutagenesis of this interesting enzyme would transform this weak, promiscuous FosX protein into a proficient GST, thus revealing the residues that are important and distinct for FosA activity versus FosX activity and illuminating the role of evolution in the development of these proteins.

Mutagenesis of *M. loti* FosX in this work was intended to elucidate residues that are important for FosA activity in distinction to FosX activity. Although creation of a

functional  $K^+$  binding loop and enhancement of GSH binding in *M. loti* FosX were not successful, these experiments revealed that there may be other structural components necessary for binding and utilizing  $K^+$  and GSH effectively. A similar idea was also proposed in studying the FosA encoded by the transposon Tn2921. Crystallization of the completely apo FosA enzyme revealed a highly flexible  $K^+$  loop region in the absence of bound  $K^+$ , while the active site and  $Mn^{2+}$  binding site did not seem to be disordered or perturbed. Perhaps even more intriguing was that  $NH_4^+$ , which is known to activate the enzyme, was present in the buffer but was unable to occupy the  $K^+$  loop region. This raises questions to whether substrate or  $Mn^{2+}$  binding must occur first in order to structurally orient the  $K^+$  binding region to form a functional  $K^+$  loop. This certainly may explain why simple insertion of  $K^+$  binding residues into FosX may not be sufficient to form a functional binding loop (27).

Alternatively, the P95K/P98R mutations may have been unsuccessful due to the requirement of a structured  $K^+$  binding loop for orienting the GSH binding site. The sequence of FosA reveals that the residues comprising the  $K^+$  binding loop are adjacent to those comprising the GSH binding residues. It is probable that without a structured  $K^+$  loop, the GSH binding site may not be oriented for effective GSH binding.

In order to transform the weak, promiscuous FosA activity of the *M. loti* FosX into a proficient GST activity, it appears that a more global approach should be taken in terms of mutating the active site or GSH binding site to mimic those of the FosA proteins.



## CHAPTER VI

### CONCLUSIONS

The FosX metalloprotein from *Brucella melitensis* has been characterized and shown to be an effective fosfomycin-hydrolysing enzyme, but it is still unclear how effective this protein is in providing resistance *in vivo*. From the MIC assays performed in *E. coli*, the *B. melitensis* FosX appears to provide no resistance to fosfomycin at all. This observation was peculiar since *in vitro*, this enzyme was as proficient as the *L. monocytogenes* FosX, which does provide robust resistance to fosfomycin. It is now apparent that the origin of this discrepancy between *in vitro* and *in vivo* activity seems to lie in the different metal preferences of the FosX proteins.

The metal binding properties of the *B. melitensis* and *C. botulinum* FosX proteins are particularly intriguing and have suggested that our model organism, *E. coli*, may not provide a mimetic intracellular environment in terms of metal availability. Metal binding kinetics have demonstrated that the *B. melitensis* and *C. botulinum* enzymes bind  $\text{Cu}^{2+}$  more tightly than  $\text{Mn}^{2+}$ . Additionally, these enzymes demonstrate better catalytic activity in the presence of  $\text{Cu}^{2+}$  rather than any other biologically relevant, divalent metal cation. The reason for this difference in metal preference is not understood at the present time. The metal binding characteristics, however, do help us to understand why our model organism *E. coli* may not be the best model to use since *E. coli* seems to possess a different Cu trafficking system. Unfortunately, the *B. melitensis* organism is categorized as a possible agent of biological warfare, making it impossible for us to work with this organism in our current environment. Therefore, we are unable to determine an appropriate MIC for this enzyme and are unsure of its biological potential. It seems rational to expect, however, that the *B. melitensis* FosX is capable of providing the *B.*

*melitensis* organism with robust resistance to fosfomycin, just as the *L. monocytogenes* FosX of similar *in vitro* activity provides *L. monocytogenes* with robust resistance—resistance that is even observable in the clinic.

The diversity of fosfomycin resistance is evidenced within members of the FosX class. At first glance, the FosX present in the genome of the soil-dwelling, nitrogen fixing microbe *Mesorhizobium loti* appeared to be a catalytically poor enzyme in comparison to other FosX members. However, deeper investigation of this enzyme revealed that its existence may be intended for something other than actual fosfomycin resistance. For example, this microbe is not a human pathogen, but it is soil dwelling and therefore would have had the potential to be exposed to the microbes that synthesize and secrete fosfomycin. However, examination of the *M. loti* genome reveals that the gene encoding FosX resides in what appears to be an uncharacterized phosphonate utilization operon. Interestingly, the *M. loti* FosX is such a catalytically poor enzyme that it is extremely inefficient at catalyzing the hydrolysis of fosfomycin *in vitro* and provides absolutely no resistance to fosfomycin in MIC assays, suggesting it may utilize an alternative phosphonate compound as substrate. Even more striking is the fact that this protein is catalytically promiscuous, being able to catalyze the FosA reaction at very low levels. Due to its weak catalytic activity and its ability to catalyze an alternate reaction at low levels, the *M. loti* FosX may represent an intermediate in the evolution of fosfomycin resistance proteins; therefore, the *M. loti* FosX became a tool by which to probe the residues necessary for the distinction between FosX and FosA activity. Although mutations intended to enhance the promiscuous FosA activity of this enzyme (through creation of a K<sup>+</sup> binding loop and enhancement of GSH binding) were not successful, this enzyme has proven to be an interesting member of the FosX class which may help illuminate the evolution of the fosfomycin resistance proteins through site-directed mutagenesis experiments.

Future work will involve total kinetic characterization of all members of the FosX class. In addition, mutagenesis of the *M. loti* FosX will turn in an alternate direction for determination of residues necessary for transforming this enzyme into a better FosX rather than a better FosA. As more bacterial genomes become available, even more pathogens harboring fosfomycin resistance proteins may become available for study, with the intent of gaining a comprehensive understanding of enzyme-mediated fosfomycin resistance. Although it is beyond the capacity of this research project, the ultimate goal is the design of biologically active inhibitors of fosfomycin resistance proteins in order to restore the clinical usefulness of fosfomycin.

## APPENDIX

**Consensus key** (see documentation for details)

- \* - single, fully conserved residue
- : - conservation of strong groups
- . - conservation of weak groups
- no consensus

CLUSTAL W (1.81) multiple sequence alignment

```

L. monocytogenes EGD      MISGLSHITLIVKDLNKTTTFLREIFNAEEIYSSGDQTFSLSKKEFFLIA
L. monocytogenes ATCC    MISGLSHITLIVKDLNKTTAFLQNI FNAEEIYSSGDKTFSLSKKEFFLIA
C. botulinum             MIERISHITFVVKNLDKTTQLFKELFNAKZVYYSGEKKHFLFKERFFIVG
M. loti                  MIEGLSHMTFIVRDLERMTRILEGVFDAREVYASDTEQFSLSREKFFLIG
B. melitensis            MVQGLSHMTFIVRDLDRMEEILTTVFDARRVYDSGAETFSLSKERFFLIG
PA1129                   MLTGLNHLTLAVADLPASIAFYRDLLGFRLEARWDQG-----AYLELG
                          *:  .*:*: * :*      :   :. .      .      :. :.

L. monocytogenes EGD      G----LWICIMEGDSL--QEQTYNHIAFRIQSEEVDEYIERIKSLGVEIK
L. monocytogenes ATCC    G----LWICIMEGDSL--QERTYNHIAFQIQSEEVDEYTERIKALGVEMK
C. botulinum             S----QWIAVMEDANI--LNRTYHHIAFKISNSDVDNYLDKIKTLNLELK
M. loti                  D----IWVAIMQGEKL--AERSYNHIAFKIDDADFDRYAERVGKGLDMR
B. melitensis            NGKEPIWIATMEGEPL--PTRTNNHVAFKIANNEYEAYLKRRIRALGLEVR
PA1129                   S----LWLCLSRREPQYGGPAADYTHYAFGLAAADFARFAAQLRAHGVREW
                          .      *:. .      * * * * : : :. :.

L. monocytogenes EGD      PERPRVEGEGRSIFYFDNHLFELHAGTLEERLKRYHE-----
L. monocytogenes ATCC    PERPRVQEGGRSIFYFDNHLFELHAGTLEERLKRYHE-----
C. botulinum             PPRRRVSGEGYSIFYFDYDNNLFELHTETLEKRLASYTKIDNI-----
M. loti                  PPRPRVEGEGRSIFYYDDNHFELHTGTLTERLARKAKGLEAAQ----
B. melitensis            EGRSRVPEGQSIFYYDDNHFELHTGTLDERLKRYGQGR-----
PA1129                   KQNR---SEGDSFYFLDPDGHRLAHSVGLRSRLAACRQAPYAGMRFAD
                          .      .** *:* ** * * . : : * * . * .** :
    
```

FosX Protein	MW	$\epsilon$	No. aa	$pk_i$
<i>B. melitensis</i>	16149	13370	140	5.92
<i>L. monocytogenes</i> (ATCC)	15570	13370	134	5.20
<i>L. monocytogenes</i> (EGD)	15654	13370	134	4.90
<i>M. loti</i>	16180	12090	140	5.29
<i>M. loti</i> (K <sup>+</sup> loop)	15874	12090	137	5.27
<i>M. loti</i> (E44G/M57S/F34Y, K <sup>+</sup> loop)	14022	13370	137	
<i>C. botulinum</i>	16396	17210	138	8.59
<i>B. suis</i>	16198	14650	140	5.92
PA1129 (FosA)	15122	26030	136	6.57

## REFERENCES

- (1) Cohen, M. L. (1992) Epidemiology of Drug Resistance: Implications for a Post-Antimicrobial Era. *Science*, 257, 1050-1055.
- (2) Walsh, C. (2003) Where will new antibiotics come from? *Nature Reviews Microbiology* 1, 65-70
- (3) Hall, B. G. (2004) Predicting the evolution of antibiotic resistance genes. *Nature Reviews Microbiology*, 2, 430-435.
- (4) Davies, J. E. (1997) Origins, acquisition, and dissemination of antibiotic resistance determinants in *Antibiotic resistance: evolution, selection, and spread*. pp 15-27. John Wiley & Sons, Chichester.
- (5) Levy, S. B.; Marshall, B. (2004) Antibacterial resistance worldwide: causes, challenges and responses. *Nature Medicine*, 10, S122-S129.
- (6) Hendlin, D., Stapely, E. O.; Jackson, M.; Wallick, H.; Miller, A. K.; Wolf, F. J.; Miller, T. W.; Chalet, L.; Kahan, F. M.; Folitz, E. L.; Woodruff, H. B. (1969) Phosphonomycin, a new antibiotic produced by strains of *Streptomyces*. *Science*, 166, 122-123.
- (7) Kahan, F. M.; Kahan, J. S.; Cassidy, P. J. (1974) The mechanism of action of fosfomycin. *Ann. NY Acad. Sci.*, 235, 364-386.
- (8) Drcmery, S.; Hromec J.; Demesova, D. (2001) Treatment of lower urinary tract infection in pregnancy. *Int. J. Antimicrob. Agents*, 17, 279-282.
- (9) Allerberger, F.; Klare, I. (1999) In-vitro activity of fosfomycin against vancomycin-resistant enterococci. *J. Antimicrob. Chemoth.*, 43, 211-217.
- (10) Ungheri, C.; Albini, E.; Belluco, G. (2002) In-Vitro Susceptibility of Quinolone-Resistant Clinical Isolates of *Escherichia coli* to Fosfomycin Trometamol. *J. Chemother.* 14, 237-240.
- (11) Kim, D. H.; Lees, W. J.; Kempell, K. E.; Lane, W. S.; Duncan, K.; Walsh, C. T. (1996) Characterization of a Cys115 to Asp substitution in the *Escherichia coli* cell wall biosynthesis enzyme UDP-GlcNAc enolpyruvyl transferase (MurA) that confers resistance to inactivation by the antibiotic fosfomycin. *Biochemistry*, 35, 4923-4928.
- (12) Tsuruoka, T.; Yamada, Y. (1975) Characterization of spontaneous fosfomycin (phosphonomycin)-resistant cells of *Escherichia coli* B in vitro. *J. Antibiot.*, 28, 906-911.

- (13) Kadner, R. J.; Winkler, H. H. (1973) Isolation and characterization of mutations affecting the transport of hexose phosphates in *Escherichia coli*. *J. Bacteriol.* 113, 895-900.
- (14) Garcia-Lobo, J. M.; Oritz, J. M. (1982) *Tn2921*, a transposon encoding fosfomycin resistance. *J. Bacteriol.*, 151, 477-479.
- (15) Llana, J.; Villar, C. J.; Salas, J. A.; Suarez, J. E.; Mendoza, M. C.; Hardisson, C. (1985) Plasmid-mediated fosfomycin resistance is due to enzymatic modification of the antibiotic. *Antimicrob. Agents Chemoth.*, 28, 163-164.
- (16) Arca, P.; Rico, M.; Brana, A. F.; Villar, C. J.; Hardisson, C.; Suarez, J. E. (1988) Formation of an adduct between fosfomycin and glutathione: a new mechanism of antibiotic resistance in bacteria. *Antimicrob. Agents Chemoth.*, 32, 1552-1556.
- (17) Armstrong, R. N. (2000) Mechanistic Diversity in a metalloenzyme superfamily. *Biochemistry*, 39, 13625-13632.
- (18) Bernat, B. A.; Laughlin, L. T.; Armstrong, R. N. (1997) Fosfomycin resistance protein (FosA) is a manganese metalloglutathione transferase related to glyoxylase I and the extradiol dioxygenases. *Biochemistry*, 36, 3050-3055.
- (19) Bernat, B. A.; Laughlin, L. T.; Armstrong, R. N. (1999) Elucidation of a monovalent cation dependence and characterization of the divalent cation binding site of fosfomycin resistance protein (FosA). *Biochemistry*, 23, 7462-7469.
- (20) Bernat, B. A.; Laughlin, L. T.; Armstrong, R. N. (1998) Regiochemical and stereochemical course of the reaction catalyzed by the fosfomycin resistance protein, FosA. *J. Org. Chem.*, 63, 3778-3780.
- (21) Fillgrove, K. L.; Pakhomova, S.; Newcomer, M. E.; Armstrong, R. N. (2003) Mechanistic diversity of fosfomycin resistance in pathogenic microorganisms. *J. Am. Chem. Soc.*, 125, 15730-15731.
- (22) Hof, H. (2003) Therapeutic options. *FEMS Immunology and Medical Microbiology*, 35, 203-205.
- (23) O'Brien, P. J.; Herschlag, D. (1999) Catalytic promiscuity and the evolution of new enzymatic activities. *Chemistry & Biology*, 6, R91-R105.
- (24) Finney, L. A., T. V. O'Halloran. (2003) Transition metal speciation in the cell: insights from the chemistry of metal ion receptors. *Science*, 300, 931-936.
- (25) Banci, L.; Bertini, I.; Ciofi-Baffoni S.; Del Conte, R.; Gonnelli, L. (2003) Understanding copper trafficking in bacteria: interaction between the

copper transport protein CopZ and N-terminal domain of the copper ATPase CopA from *Bacillus subtilis*. *Biochemistry*, 42, 1939-1949.

- (26) Jordan, I. K.; Natale, D. A.; Koonin, E. V.; Galperin, M. Y. (2001) Independent evolution of heavy metal associated domains in copper chaperones and copper-transporting ATPases. *J. Mol. Evol.*, 53, 622-633.
- (27) Pakhomova, S.; Rife, C. L.; Armstrong, R. N.; Newcomer, M. E. (2004) Structure of fosfomycin resistance protein FosA from transposon *Tn2921*. *Protein Science*, 13, 1260-1265.